



**HAL**  
open science

## The neural basis of rapid unfamiliar face individuation with human intracerebral recordings

Corentin Jacques, Bruno Rossion, Angélique Volfart, Hélène Brissart, Sophie Colnat-Coulbois, Louis Maillard, Jacques Jonas

► **To cite this version:**

Corentin Jacques, Bruno Rossion, Angélique Volfart, Hélène Brissart, Sophie Colnat-Coulbois, et al.. The neural basis of rapid unfamiliar face individuation with human intracerebral recordings. *NeuroImage*, 2020, 221, pp.117174. 10.1016/j.neuroimage.2020.117174 . hal-03437720

**HAL Id: hal-03437720**

**<https://hal.science/hal-03437720>**

Submitted on 20 Nov 2021

**HAL** is a multi-disciplinary open access archive for the deposit and dissemination of scientific research documents, whether they are published or not. The documents may come from teaching and research institutions in France or abroad, or from public or private research centers.

L'archive ouverte pluridisciplinaire **HAL**, est destinée au dépôt et à la diffusion de documents scientifiques de niveau recherche, publiés ou non, émanant des établissements d'enseignement et de recherche français ou étrangers, des laboratoires publics ou privés.



Distributed under a Creative Commons Attribution 4.0 International License



# The neural basis of rapid unfamiliar face individuation with human intracerebral recordings

Corentin Jacques<sup>a,1</sup>, Bruno Rossion<sup>a,b,c,1,\*</sup>, Angélique Volfart<sup>a,b</sup>, Hélène Brissart<sup>b,c</sup>,  
Sophie Colnat-Coulbois<sup>b,d</sup>, Louis Maillard<sup>b,c</sup>, Jacques Jonas<sup>b,c</sup>

<sup>a</sup> Psychological Sciences Research Institute and Institute of Neuroscience, Université Catholique de Louvain (UCLouvain), 1348 Louvain-la-Neuve, Belgium

<sup>b</sup> Université de Lorraine, CNRS, CRAN, F-54000 Nancy, France

<sup>c</sup> Université de Lorraine, CHRU-Nancy, Service de Neurologie, F-54000 Nancy, France

<sup>d</sup> Université de Lorraine, CHRU-Nancy, Service de Neurochirurgie, F-54000 Nancy, France

## ARTICLE INFO

### Keywords:

Face recognition

SEEG

Fast periodic visual stimulation

Ventral occipito-temporal cortex

Fusiform gyrus

## ABSTRACT

Rapid individuation of conspecifics' faces is ecologically important in the human species, whether the face belongs to a familiar or unfamiliar individual. Here we tested a large group ( $N = 69$ ) of epileptic patients implanted with intracerebral electrodes throughout the ventral occipito-temporal cortex (VOTC). We used a frequency-tagging visual stimulation paradigm optimized to objectively measure face individuation with direct neural recordings. This enabled providing an extensive map of the significantly larger neural responses to upright than to inverted unfamiliar faces, i.e. reflecting visual face individuation processes that go beyond physical image differences. These high-level face individuation responses are both distributed and anatomically confined to a strip of cortex running from the inferior occipital gyrus all along the lateral fusiform gyrus, with a large right hemispheric dominance. Importantly, face individuation responses are limited anteriorly to the bilateral anterior fusiform gyrus and surrounding sulci, with a near absence of significant responses in the extensively sampled temporal pole. This large-scale mapping provides original evidence that face individuation is supported by a distributed yet anatomically constrained population of neurons in the human VOTC, and highlights the importance of probing this function with face stimuli devoid of associated semantic, verbal and affective information.

## 1. Introduction

Face individuation (FID) occurs when the face of a unique individual elicits a specific behavioral and/or neural response that is reliably distinct from the response to other individuals. Individuation of *unfamiliar* faces is critical in the human species for three main reasons. First, in humans, recognition of conspecifics' identity is based primarily on the face (Sheehan and Nachman, 2014). Second, in most human societies, people are constantly exposed to unfamiliar faces in their natural or digital environment. Third, recognizing familiar people based on their faces requires to pick out idiosyncratic features of these faces when we first encounter them or when they have not yet been encoded in long-term memory, i.e. when they are unfamiliar.

Although non-human animal species can be trained to behaviorally individuate pictures of unfamiliar faces of conspecifics or even of humans, their performance is often limited and strictly image-dependent (e.g., fish: Newport et al., 2016; wasps: Sheehan and Tibbetts, 2011).

By comparison, human adults naturally excel at individuating unfamiliar human faces (Rossion, 2018), having acquired this ability without formal training throughout development (Carey, 1992; Hills and Lewis, 2018). Their individuation of unfamiliar faces is fast (e.g., within 1–2 fixations and a few hundreds of milliseconds; Hsiao and Cottrell, 2008; Jacques et al., 2007) and automatic (i.e., occurring without the intention to do so and being able to suppress it; Liu-Shuang et al., 2014; Palermo and Rhodes, 2007; Yan et al., 2019).

Given the importance of faces for social interactions in the human species, understanding the neural basis of human FID must be a major scientific goal in cognitive neuroscience. Using pictures of unfamiliar faces is critical to achieve this goal since they are not associated with semantic information, affect or verbal labels, therefore allowing to isolate the contribution of *visual* processes to FID (Rossion, 2018). Neurophysiological studies have reported face-selective neurons in the infero-temporal cortex of the macaque monkey that fire at a different spike rate to pictures of different (monkey and human) unfamiliar

\* Corresponding author at: CRAN, UMR 7039, CNRS - Université de Lorraine, Pavillon Krug, Hôpital Central, CHRU Nancy - University Hospital of Nancy, 29 Avenue du Maréchal de Lattre de Tassigny, 54000 Nancy, France.

E-mail address: [bruno.rossion@univ-lorraine.fr](mailto:bruno.rossion@univ-lorraine.fr) (B. Rossion).

<sup>1</sup> These authors contributed equally

faces, suggesting that face identity is coded in terms of distributed patterns of spike rates in small local neuronal populations (Baylis et al., 1985; Chang and Tsao, 2017; Leopold et al., 2006; also Young and Yamane, 1992 with familiar faces). However, similarly to other non-human animal species, macaque monkeys are poor at behavioral FID tasks and may rely essentially on low-level image-based statistics (Parr et al., 2008; Rossion and Taubert, 2019). Moreover, their performance differ qualitatively from humans at such tasks (e.g., no effect of picture-plane inversion of the stimuli; see Bruce, 1982; Griffin, 2020) such that this species does not provide an adequate model of human FID (Rossion and Taubert, 2019). In humans, neurons firing for specific facial identities have been recorded in the medial temporal lobe, but this firing occurs only to highly familiar faces, irrespective of the presentation format (e.g., Jennifer Aniston's face and her written name) (Quian Quiroga et al., 2005). Moreover, these neurons fire relatively late (about 300 ms onset) and are thought to play a role in recollecting conscious episodic multimodal memory events rather than in the FID process *per se* (Quian Quiroga, 2012; Rey et al., 2020).

At the system level of neural organization in humans, lesions causing a selective impairment in face identity recognition, i.e. prosopagnosia (Bodamer, 1947), are located in the ventral occipito-temporal cortex (VOTC), with a right hemispheric lesion being both necessary and sufficient to cause such impairment in most individuals (Barton, 2008; Bouvier and Engel, 2006; Meadows, 1974; Sergent and Signoret, 1992). Providing that correct response times are considered, these patients are also systematically impaired at unfamiliar face matching tasks (Farah, 1990). While the brain structures involved remain necessarily coarsely defined in lesion studies, recent studies have reported that focal intracerebral stimulation of the face-selective regions in the right VOTC generate transient impairments in face identity recognition (Jonas et al., 2015, 2012), including unfamiliar face matching (Jonas et al., 2014). In typical adults, functional magnetic resonance imaging (fMRI) studies have used fMRI-adaptation and multivariate pattern analysis (MVPA) to define the neural basis of FID. On the one hand, fMRI-adaptation takes advantage of the reduced neural response to a repeated stimulus ('repetition suppression') (Grill-Spector et al., 2006; Grill-Spector and Malach, 2001). Repetition suppression effects for unfamiliar individual face pictures have been found in pre-defined face-selective regions of the VOTC such as the inferior occipital gyrus (IOG, or "Occipital Face Area", OFA) and the lateral section of middle fusiform gyrus (latFG or "Fusiform Face Area", FFA; Eger et al., 2004; Ewbank et al., 2013; Gauthier et al., 2000; Gilaie-Dotan et al., 2010; Hermann et al., 2017; Hughes et al., 2019; Rostalski et al., 2019; Schiltz and Rossion, 2006). On the other hand, MVPA approaches rely on the decoding of differences between the patterns of activity evoked by different individual faces across multiple voxels. However, the decoding accuracies in this approach, often for simple image-based discriminations, are rather modest and found in inconsistent brain regions across studies (Anzellotti et al., 2014; Goesaert and Op de Beeck, 2013; Kriegeskorte et al., 2007; Natu et al., 2010; Nestor et al., 2011; see the critical view in Kanwisher, 2017).

Overall, fMRI studies have either focused on specific regions of interest or investigated response patterns at a local scale (i.e., region-of-interest analyses in repetition suppression; searchlight analyses in MVPA), rather than considering the whole VOTC. Similarly, the majority of human intracranial EEG studies that have investigated FID using repetition suppression (Engell and McCarthy, 2014; Puce et al., 1999) or MVPA (Davidesco et al., 2014; Ghuman et al., 2014) have either focused on specific anatomical regions (Davidesco et al., 2014; Engell and McCarthy, 2014; Ghuman et al., 2014; see Puce et al., 1999 for an exception) or combined data from different regions (Davidesco et al., 2014). In addition, despite its strengths (i.e., non-invasiveness, high spatial resolution and large spatial coverage), fMRI provides indirect neural recordings associated with large fluctuations of signal-to-noise ratio across brain regions, making it difficult to fairly assess the FID function across the entire VOTC. In particular, due to severe magnetic susceptibility ar-

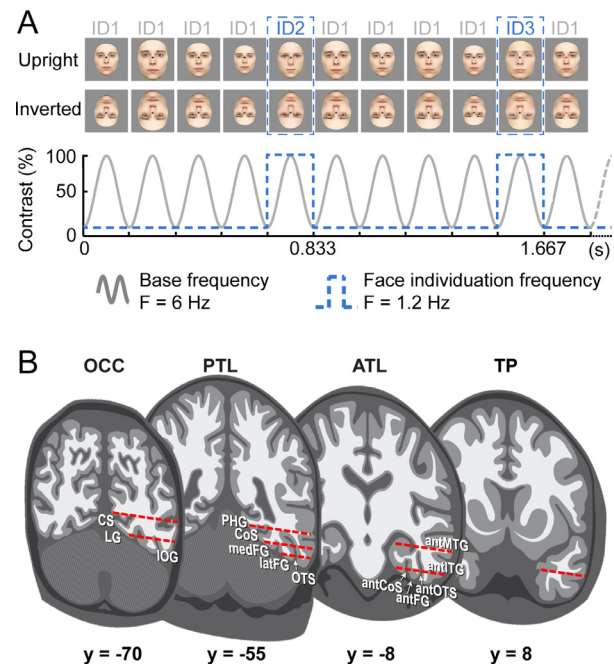


**Fig. 1.** Fast periodic visual stimulation (FPVS) paradigm and SEEG method. **A.** In the paradigm used here (from Liu-Shuang et al., 2014), face images are presented by sinusoidal contrast modulation at a rate of six stimuli per second (6 Hz) in sequences of 65 s. In each sequence, a base face (here ID1) is randomly selected within a pool of 25 male or 25 female faces and repeated throughout the sequence. At a fixed interval of every 5th base face (i.e. at the frequency of  $6 \text{ Hz}/5 = 1.2 \text{ Hz}$ ), a different unfamiliar facial identity (selected from the 24 remaining faces of the same gender) is presented (e.g. ID2, ID3, etc.). To avoid pixel-wise overlap, face size is randomly varied between 77% and 123% at every stimulation cycle. In a given sequence, faces are either presented all upright or all in the inverted orientation. **B.** Schematic coronal representation of the typical trajectories of depth electrodes implanted in the VOTC. Electrodes consist of 8–15 contiguous recording contacts (red rectangles) spread along the electrode length, along the medio-lateral axis. Acronyms: TP: temporal pole; ATL: anterior temporal lobe; PTL: posterior temporal lobe; OCC: occipital lobe; PHG: parahippocampal gyrus; CoS: collateral sulcus; FG: fusiform gyrus; ITG: inferior temporal gyrus; MTG: middle temporal gyrus; OTS: occipito-temporal sulcus; CS: calcarine sulcus; IOG: inferior occipital gyrus; LG: lingual gyrus; ant: anterior; lat: lateral; med: medial. (For interpretation of the references to colour in this figure legend, the reader is referred to the web version of this article.)

tifacts arising from the ear canals (Axelrod and Yovel, 2013; Jonas et al., 2015; Rossion et al., 2018; Wandell, 2011), fMRI is limited in exploring VOTC regions located anteriorly to the middle fusiform gyrus, i.e. in the anterior temporal lobe (ATL). Although intracranial EEG studies do not suffer from regional variations in signal-to-noise ratio, previous investigations have not localized, quantified, and compared FID neural responses across anatomical regions of the human VOTC.

Here, we provide a comprehensive map of direct neural responses of FID measured in the whole human VOTC. To achieve this, we use a validated frequency-tagging paradigm to capture the FID function in a large group ( $N = 69$ ) of epileptic patients implanted with intracerebral (i.e., depth) electrodes across the VOTC (stereotaxic-electroencephalography, SEEG, Talairach and Bancaud, 1973), allowing to measure local neural activity from the cortex. In this paradigm (Liu-Shuang et al., 2014, reviewed in Rossion et al., 2020), the picture of an unfamiliar face identity devoid of external features ("base face" = ID1) is randomly selected from a large set of face identities, and repeated at a constant rate of 6 Hz for about one minute. During this face stimulation sequence, other unfamiliar face identities (ID2, ID3, ID4, etc.) are inserted among the base face at regular intervals as every 5th face (Fig. 1A). As a result, a change of face identity occurs periodically at  $6 \text{ Hz}/5$ , i.e. 1.2 Hz, while

observers complete an orthogonal task. Responses measured in the EEG (on the scalp) or SEEG (inside the brain) exactly at the 1.2 Hz identity change frequency and its harmonics (i.e., 2.4 Hz, etc.) index FID. Combined with electroencephalography, this paradigm has many advantages: it is highly sensitive (i.e., high signal-to-noise ratio and significant effects in >90% of individuals tested during a few minutes), objective (i.e., providing responses at experimentally-defined frequencies), and reliable (i.e., with stable responses within and between recording sessions, [Dzhelyova et al., 2019](#); see [Rossion et al., 2020](#) for an extensive review of 20 published studies with this paradigm with scalp EEG recordings).

Here, we extensively cover the bilateral VOTC by sampling a total of 3825 recording contacts in the gray matter from 69 participants tested with this paradigm ([Fig. 1B](#)). We quantify the 1.2 Hz FID response at each recording contact and map this response across the VOTC to define the neural basis of human unfamiliar FID. Importantly, in order to isolate high-level FID effects, i.e. effects that go beyond mere physical differences between images, we compare the FID responses to upright and inverted faces tested in separate stimulation sequences. Since picture-plane inversion is known to largely impair FID ([Yin, 1969](#); [Rossion, 2008](#) for review) and severely reduces scalp EEG responses in the paradigm used here ([Liu-Shuang et al., 2014](#)), we expect this manipulation to substantially decrease the FID response in the critical regions subtending face individuation.

## 2. Materials and methods

### 2.1. Participants

The study included 69 participants (32 females, mean age:  $32.3 \pm 8$  years, 63 right-handed and 6 left-handed) undergoing clinical intracerebral evaluation with depth electrodes (SEEG, [Talairach and Bancaud, 1973](#)) for refractory partial epilepsy in the Epilepsy Unit of the University Hospital of Nancy. They were included in the study if they had at least one intracerebral electrode implanted in the ventral occipito-temporal cortex. All participants tested in SEEG gave written consent to participate to the study, which was part of a protocol approved by the human investigation committee of the University Hospital of Nancy.

Intellectual efficiency (IQ, WAIS-IV) was assessed in 58 participants, with an average IQ score of  $88.8 \pm 14.8$ . All but 11 participants performed the electronic version of the Benton Face Recognition Test (BFRT-c; [Rossion and Michel, 2018](#); see [Benton and Van Allen, 1968](#) for the original version of the test) before the SEEG exploration. Their average score at the BFRT-c was of  $42.1 \pm 4.5$ , although 13 participants had scores below normal range (i.e., <39; range 32–52; see distribution of BFRT-c scores in [Fig. S1](#)). Average response time to perform the BFRT-c was about 6 min ( $360.4 \pm 165.8$ , range 146–1016 s; see distribution of BFRT-c reaction times in [Fig. S1A](#)). A subset of these participants ( $N = 32$ ; 46%) also performed a behavioral delayed matching task (as described in [Busigny and Rossion, 2010](#), experiment 4) with upright and inverted faces. Accuracy and response times were comparable to older control participants reported in the literature ([Busigny and Rossion, 2010](#)) and response times were correlated with age, IQ and visuospatial processing speed (as assessed by the subtest Code of the WAIS) ([Table S1](#)). They displayed a large face inversion effect in accuracy (upright faces:  $87 \pm 9.5\%$ ; inverted faces:  $71.4 \pm 11.6\%$ , one-tailed  $t$ -test:  $t(31) = 10.2$ ,  $p < 0.001$ ) and correct response times (upright faces:  $1959 \pm 480$  ms; inverted faces:  $2219 \pm 496$  ms, one-tailed  $t$ -test:  $t(31) = 6.3$ ,  $p < 0.001$ ). Every single participant of this subsample showed better performance for upright than inverted faces ([Fig. S1B](#)).

### 2.2. Intracerebral electrode implantation and SEEG recording

Intracerebral electrodes (Dixi Medical, Besançon, France) were stereotactically implanted in the patient's brain for purely clinical pur-

poses, i.e., in order to delineate the seizure onset zone ([Talairach and Bancaud, 1973](#)). The sites of electrode implantation were determined based on non-invasive data collected during an earlier phase of the investigation. Each 0.8 mm diameter intracerebral electrode contains 8–15 independent recording contacts of 2 mm in length separated by 1.5 mm from edge to edge ([Fig. 1B](#), for details about the electrode implantation procedure, see [Salado et al., 2018](#)). The exact anatomical location of each recording contact was determined by coregistration of post-operative non-stereotactic CT-scan with a pre-operative T1-weighted MRI. A total of 484 electrode arrays were implanted in the VOTC of the 69 participants. These electrodes contained 3825 individual recording contacts in the gray matter (left hemisphere: 2031; right hemisphere: 1794). Intracerebral EEG was recorded at a 512 Hz sampling rate referenced to either a midline prefrontal scalp electrode (FPz, in 59 participants) or an intracerebral contact in the white matter (in 10 participants).

### 2.3. Face individuation fast periodic visual stimulation (FPVS) paradigm

#### 2.3.1. Stimuli

We used full-front colored photographs of 25 male and 25 female faces with a neutral expression, taken under standardized conditions with respect to lighting, background, and distance from the camera ([Fig. 1A](#) for examples of faces; same stimuli as in [Liu-Shuang et al., 2014](#)). External features such as hair and ears were cropped out. Inverted (upside-down) versions of these faces were generated by vertically flipping each image.

#### 2.3.2. Experimental procedure

Participants viewed sequences of face images ([Fig. 1A](#)) presented at a rate of 6 Hz through sinusoidal contrast modulation. In separate sequences, faces were either presented in the upright orientation or in the inverted orientation. Faces were of the same sex within a sequence. A sequence lasted 65 s, consisting of 60 s of stimulation at full-contrast followed by 5 s of “fade-out”, where contrast gradually decreased. In every sequence, the base face was one randomly selected face identity (within the 25 faces of one sex set) and repeated throughout at 6 Hz (e.g., identity 1, ID1). At fixed intervals of every 1/5 face, a different facial identity (selected from the 24 remaining faces of the same sex set) was shown (ID2, ID3, ID4, etc.). Thus, face identity changes occurred at a frequency of 6 Hz/5, i.e., 1.2 Hz ([Fig. 1A](#)). As a result, EEG amplitude at this frequency (1.2 Hz) and its harmonics (i.e. integer multiples: 2.4 Hz, 3.6 Hz, etc.) was used as an index of the visual system's discrimination of individual faces. To avoid confounding changes of face identity with changes of local pixel intensity (e.g., blue eyes vs. brown eyes), face size varied randomly between 77% and 123% at every 6 Hz stimulation cycle to minimize the overlap between the spatial location of a given facial landmark across cycles. During the stimulation, participants fixated a small black cross presented continuously at the center of the stimuli and had to detect brief (500 ms) color-changes of this fixation cross (black to red), occurring randomly 8 times in each sequence. Due to equipment malfunction, the behavioral data at color-change detection is missing for 11 participants. In the remaining 58 participants, accuracy at detecting the color change of the fixation cross was near ceiling for both the upright ( $96.7 \pm 4.3\%$ ; range: 61 to 100%) and inverted ( $95.1 \pm 5.7\%$ ; range: 60 to 100%) conditions, with no significant difference between conditions ( $p = 0.2$ , 2-tailed paired permutation test). Participants were slightly and significantly slower to respond to the color change in the upright ( $471 \pm 56$  ms) compared to inverted ( $457 \pm 50$  ms) condition ( $p = 0.011$ , 2-tailed paired permutation test).

Half of the participants ( $N = 34$ ) were presented with 4 sequences (2 sequences per face orientation, one with male faces, one with female faces, i.e. around 5 min of experiment, including short breaks). Twenty-two participants viewed 8 sequences (4 in each face orientation), 3 participants viewed 12 sequences (6 per face orientation) and 10 participants viewed only 2 sequences (1 per face orientation). These

differences across participants were due to the particular clinical context in which the experiment took place. Since the study does not compare across individual participants, we considered all the collected data for analysis. No participant had seizures in the 2 h preceding FPVS recordings.

#### 2.4. SEEG signal processing and analyses

SEEG signal processing and analyses were largely similar to those in previous studies with this approach (Jonas et al., 2016; Lochy et al., 2018) but is reported in full in the present study.

##### 2.4.1. Frequency domain processing

We analyzed segments of SEEG corresponding to stimulation sequences (69-second segments,  $-2$  s to  $+67$  s). The 69 s data segments were cropped to contain an integer number of 1.2 Hz cycles beginning 2 s after the onset of the sequence until approximately 60 s, before stimulus fade-out (69 identity change cycles  $\approx$  58 s). Sequences were then averaged in the time-domain, separately for each condition and each participant. No further pre-processing was applied to the recordings. Subsequently, a Fast Fourier Transform (FFT) was applied to these averaged segments and amplitude spectra (see examples in Fig. 2A) were extracted for all contacts.

##### 2.4.2. Face individuation (FID) responses

The FPVS approach used here allows identifying two distinct types of responses: (1) a general visual stimulation response at the base stimulation frequency (6 Hz) and its harmonics (e.g., 12 Hz, 18 Hz, etc.), as well as (2) a face individuation response at 1.2 Hz and its harmonics (FID response, Fig. 1A). In the current study, we will focus on the FID response. The significance of FID responses relative to noise was determined as follows (Fig. 2). First, the FFT spectrum was cut into segments centered at the identity change frequency and harmonics, i.e., 1.2 Hz, 2.4 Hz, 3.6 Hz and 4.8 Hz (no responses were found above 6 Hz) and surrounded by 25 neighboring bins on each side. Next, the amplitude values of these 4 segments of FFT spectra were summed. Finally, the summed FFT spectrum was transformed into a Z-score. Z-scores were computed as the difference between the amplitude at the center identity change frequency bin and the mean amplitude of 48 surrounding bins (25 bins on each side, excluding the 2 bins directly adjacent to the bin of interest, i.e., 48 bins), divided by the standard deviation of amplitudes in the corresponding 48 surrounding bins. A recording contact was labeled as an FID contact if the Z-score of the FID response at the identity change frequency bin exceeded 3.1 (i.e.,  $p < 0.001$  one-tailed), in the upright, in the inverted condition or in both conditions. A one-tailed test was used as the search is restricted to recording contacts showing larger signal than noise (Dzhelyova et al., 2019; Jonas et al., 2016; Liu-Shuang et al., 2016; Lochy et al., 2018).

##### 2.4.3. Classification of FID contacts in UP and INV contacts

For the proportion analysis, FID contacts were further split in 2 sets of contacts: (1) the contacts that showed a significant FID response in the upright condition, regardless of the responses in the inverted condition (UP contacts, Fig. 3, left); (2) the contacts that showed a significant FID response in the inverted condition, regardless of the responses in the upright condition (INV contacts, Fig. 3, right). Some contacts exhibited significant responses in both upright and inverted conditions such that the two sets overlapped (Fig. 3, bottom; Fig. 4A).

##### 2.4.4. Quantification of response amplitude

Amplitude quantification was performed on all FID contacts (i.e., significant FID response either for upright or inverted condition) independently for the upright and inverted conditions, following a similar procedure as described above for defining significant contacts. Specifically, we first computed baseline-subtracted amplitudes in the frequency domain as the difference between the amplitude at each frequency bin

**Table 1**

Number of contacts showing significant FID responses (in upright and/or inverted conditions) in each anatomical region. The corresponding number of subjects in which these contacts were found is indicated in parenthesis. For each region, the larger anatomical subdivision is indicated in parenthesis. Acronyms: VMO: ventro-medial occipital cortex; IOG: inferior occipital gyrus; medFG: medial fusiform gyrus and collateral sulcus; latFG: lateral fusiform gyrus and occipito-temporal sulcus; MTG/ITG: the inferior and middle temporal gyri; antCoS: anterior collateral sulcus; antOTS: anterior occipito-temporal sulcus; antFG: anterior fusiform gyrus; antMTG/ITG: anterior middle and inferior temporal gyri; TP: temporal pole; OCC: occipital lobe; PTL: posterior temporal lobe; ATL: anterior temporal lobe.

Regions	Left hemisphere	Right hemisphere
VMO (OCC)	23 (4)	15 (5)
IOG (OCC)	11 (5)	33 (8)
medFG (PTL)	11 (7)	16 (6)
latFG (PTL)	22 (10)	33 (9)
MTG/ITG (PTL)	1 (1)	4 (3)
antCoS (ATL)	12 (7)	14 (9)
antFG (ATL)	6 (4)	15 (6)
antOTS (ATL)	23 (11)	10 (4)
antMTG/ITG (ATL)	19 (6)	13 (6)
TP	10 (3)	4 (3)
Total	138	157

and the average of 48 corresponding surrounding bins (up to 25 bins on each side, i.e., 50 bins, excluding the 2 bins directly adjacent to the bin of interest, i.e., 48 bins). Then, FID response amplitude was quantified for each significant FID contact as the sum of the baseline-subtracted amplitudes at the first 4 harmonics of the identity change frequency (i.e. 1.2, 2.4, 3.6 and 4.8 Hz). Amplitude was quantified independently for the upright and inverted conditions. In addition, the effect of face inversion was computed for each contact as the amplitude difference between upright and inverted conditions. Contacts located in the same individually defined anatomical region (see section ‘‘Contact localization in the individual anatomy’’ below) were grouped, separately for the left and the right hemisphere. In each anatomical region, we statistically compared group-level FID amplitude differences between hemispheres using general linear mixed effect models implemented in the lme4 package (Bates et al., 2015) in R v4.0.0. Statistical models were fitted using REML and  $p$ -values were obtained using Satterthwaite’s approximation for degrees of freedom. Models included a random intercept per participant to account for both inter-participants variability and non-independence of contacts within a participant. The significance of the face inversion effect was tested at group-level for each region and each hemisphere by comparing amplitudes in the upright vs. inverted conditions using general linear mixed effect models with a random intercept for factors ‘contacts’ nested in ‘participants’. Each set of tests was corrected for multiple comparisons using Benjamini-Hochberg false discovery rate correction (Benjamini and Hochberg, 1995). Note that the FID responses amplitude quantification in the middle temporal gyrus and inferior temporal gyrus (MTG/ITG) and temporal pole were not performed as there were too few contacts in these regions to obtain reliable measures (Table 1).

#### 2.5. Contact localization in the individual anatomy

The exact position of each contact relative to brain anatomy was determined in each participant’s own brain by coregistering the post-operative CT-scan with a T1-weighted MRI of the patient’s head. Contacts located in the white matter were excluded from the analyses. To accurately assign an anatomical label to each contact, we used the same topographic parcellation of the VOTC as in Jonas et al. (2016) and Lochy et al. (2018), which is close to the parcellation proposed by Kim et al. (2000). Major VOTC sulci (collateral sulcus, CoS; midfusiform sul-

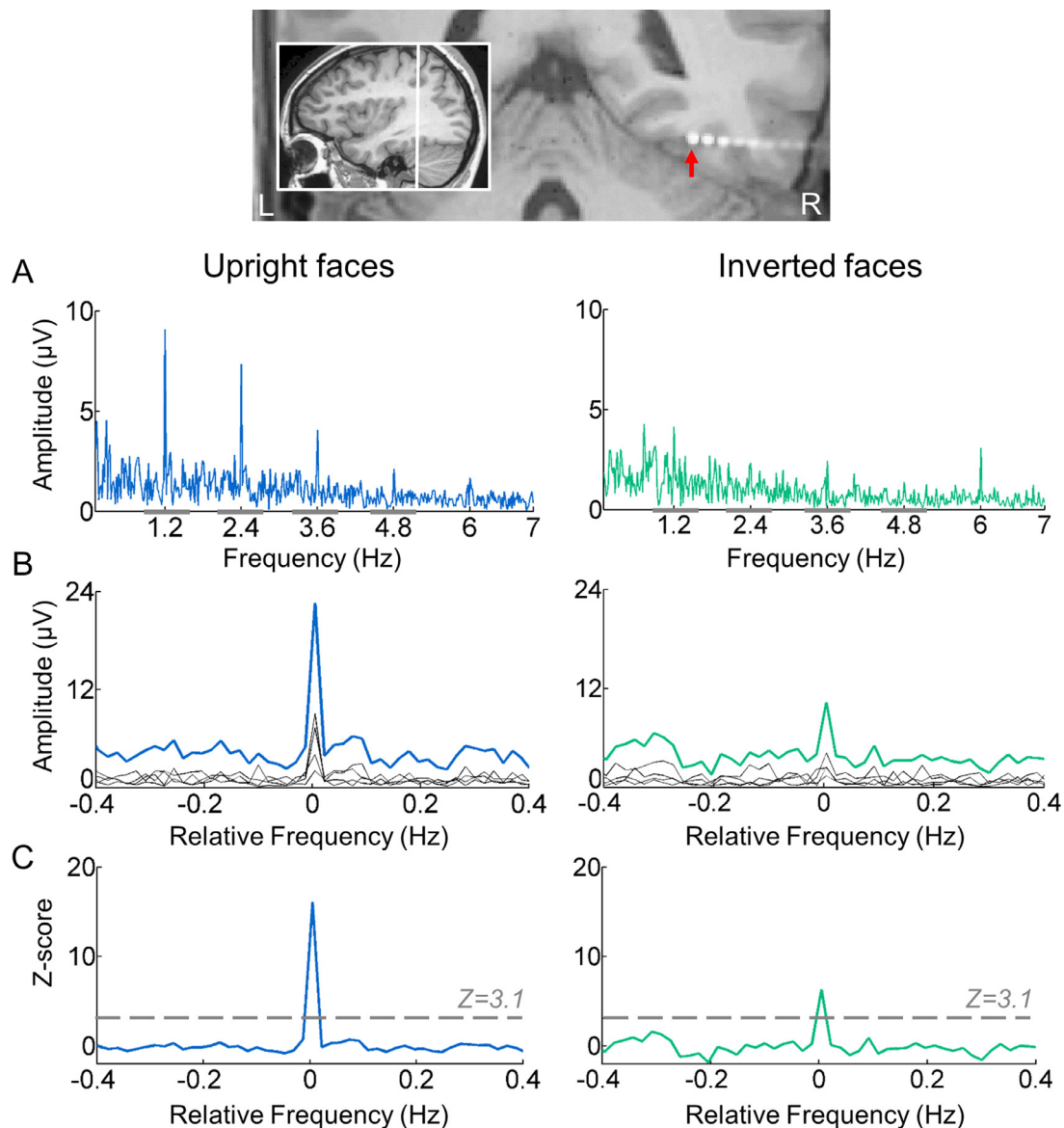


**Fig. 2.** Objective and high signal-to-noise ratio FID responses recorded in the VOTC. **A.** SEEG frequency-domain responses recorded at an individual recording contact in the upright (left) and inverted (right) conditions. The anatomical location of the contact (in the right latFG) is shown in a coronal MRI slice (indicated by a red arrow). FID responses are found at the exact face identity change frequency and harmonics (1.2, 2.4, 3.6, and 4.8 Hz) in both upright and inverted conditions, albeit with a higher amplitude in the upright condition. **B.** Significant selective responses were determined by first segmenting the FFT spectrum into four segments centered at the frequency of face identity change and its harmonics up to 4.8 Hz. Individual FFT segments are shown in gray (see horizontal gray bars on the X axis in A, representing the length of each FFT segment). The four segments, containing both the signal and the surrounding noise, were then summed (colored line). The 0 mark corresponds to the face identity change frequency. **C.** Z-score transformation of the summed FFT spectrum for statistical purpose and computed as the difference between the amplitude at the identity change frequency bin and the mean amplitude of 48 surrounding bins (25 bins on each side, excluding the 2 bins directly adjacent to the bin of interest, i.e., 48 bins), divided by the standard deviation of amplitudes in the 48 surrounding bins. The Z score at the face identity change frequency exceeds 3.1 ( $p < 0.001$ ) in the upright condition (left) and in the inverted condition (right). This contact was therefore classified as an UP contact and as an INV contact. (For interpretation of the references to colour in this figure legend, the reader is referred to the web version of this article.)

cus, MFS; and occipito-temporal sulcus, OTS) served as medio-lateral landmarks while coronal reference planes containing given landmarks served as postero-anterior landmarks (Fig. S2). A coronal plane including the anterior tip of the parieto-occipital sulcus served as the border of the occipital lobe (OCC) and posterior temporal lobe (PTL). A coronal plane including the posterior tip of the hippocampus served as the border between the PTL and the anterior temporal lobe (ATL). A coronal plane including the limen insulae served as the border between the ATL and the temporal pole (TP). Hence, we located contacts in the ATL if they were located anteriorly to the posterior tip of the hippocampus (i.e., anteriorly to a Y Talairach coordinate around  $-40$ ) and posteriorly to the limen insulae.

## 2.6. Group visualization, proportion and amplitude analyses in Talairach space

For group analyses and visualization, anatomical MRI were spatially normalized in order to determine the Talairach coordinates of VOTC intracerebral contacts. The cortical surface used to display group maps was obtained from segmenting the Colin27 brain from AFNI (Cox, 1996), which is aligned to the Talairach space. We performed two separate group analyses using Talairach transforms.

First, we used Talairach transformed coordinates to compute the local proportion of FID intracerebral contacts across the VOTC. Unlike in the amplitude quantification analysis, proportions were computed

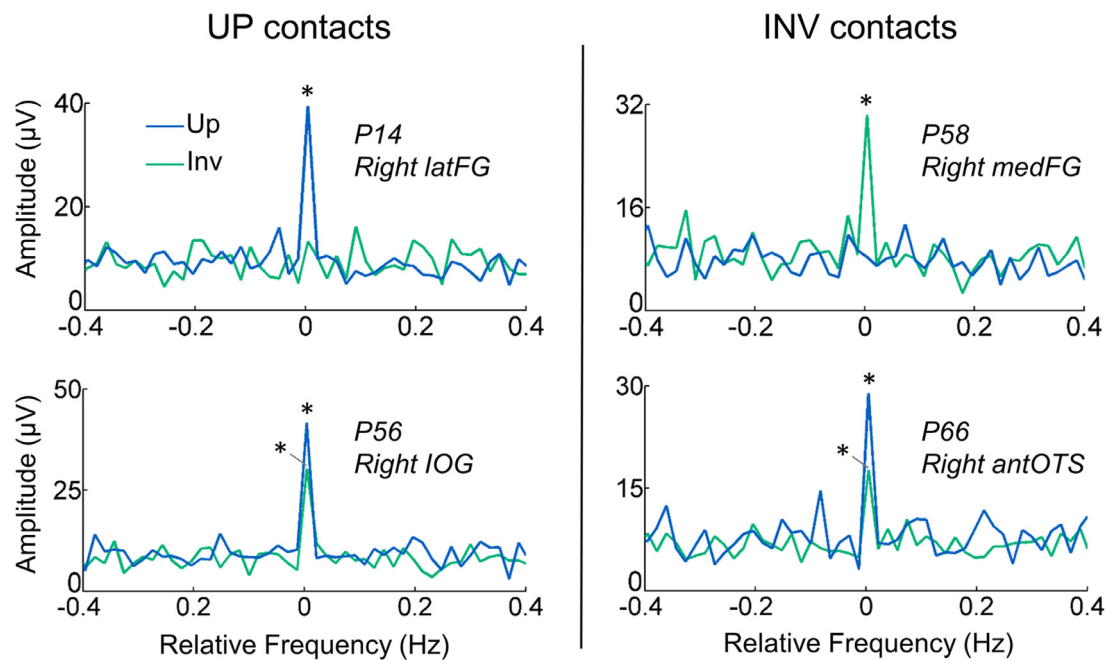


**Fig. 3.** Classification of FID contacts in UP and INV contacts for the proportion analysis. Example of summed segmented FFT spectra for the upright and inverted conditions in 4 recording contacts, illustrating the classification of FID contacts in UP and INV contacts (left and right columns respectively). Top-row: Contacts significant only either in the upright (left, UP contacts) or in the inverted (right, INV contacts) conditions. Bottom row: example contacts with a significant FID response in both conditions being classified as both UP and INV contacts. \* Indicates statistically significant responses ( $Z > 3.1$ ,  $p < 0.001$ ).

separately for UP contacts (i.e. contacts with significant FID response in the upright condition, independently of the inverted condition) and INV contacts (i.e. contacts with significant FID response in the inverted condition, independently of the upright condition). For ventral views of the VOTC, local proportion of contacts was computed in volumes (i.e. ‘voxels’) of size  $15 \times 15 \times 100$  mm (respectively for the X: left – right, Y: posterior – anterior, and Z: inferior – superior dimensions) by steps of  $3 \times 3 \times 100$  mm over the whole VOTC. A large voxel size in the Z dimension enabled collapsing across contacts along the inferior-superior dimension, in order to increase statistical power and provide a compact visualization of the VOTC. Additional views of the lateral VOTC were generated by running the same analyses using voxels of size  $20 \times 20 \times 15$  mm by steps of  $3 \times 3 \times 3$  mm along the X, Y and Z dimensions respectively. For each voxel, we extracted the following information across all participants in our sample: (1) number of recorded contacts located within the voxel; (2) number of significant UP and INV contacts. From these values, for each voxel we computed the proportion of significant contacts as the number of UP or INV contacts within the voxel divided by the total number of recorded contacts located in that voxel. Then, for each voxel we determined whether the proportions of significant UP or INV contacts were significantly above zero using a bootstrap procedure, as follows: (1) within each voxel, sample as many contacts as the number of recorded contacts, with replacement; (2) for this bootstrap sample, determine the proportion of UP or INV contacts and store this value; (3) repeat steps (1) and (2) 5000 times to generate a distribution of bootstrap proportions; and (4) estimate the  $p$ -value as the fraction of bootstrap proportions equal to zero. In addition, we statistically compared the proportion VOTC maps for UP vs. INV contacts in the same manner as described above but using, for each voxel, the difference between the number of UP vs. INV contacts in relation to the number of recorded contacts. With the UP vs. INV difference map, we also statistically determined interhemispheric differences by comparing this UP-INV difference of proportion across corresponding voxels of the left vs. right hemispheres, again using a permutation test.

Second, we used the same mapping approach to compute the local FID response amplitude across the VOTC. Here, we plotted the mean

baseline-subtracted amplitude across all the FID contacts (i.e. responding significantly either in the upright or inverted conditions) within each  $15 \times 15 \times 100$  mm voxel (for the ventral view) or  $20 \times 20 \times 15$  mm (for the lateral view) over the cortical surface. Mapping the FID response amplitude in the upright and inverted conditions therefore uses the same set of contacts. We also statistically compared the amplitude maps for upright and inverted conditions by applying a paired-sample permutation test (2-tailed, 5000 permutations) to the amplitude in the sample of contacts within each voxel.

### 3. Results

#### 3.1. Spatial distribution of face individuation (FID) contacts in the VOTC

Following Fast Fourier Transform of SEEG data, high signal-to-noise FID responses were identified in the VOTC at exactly the identity change frequency (1.2 Hz) and harmonics (Fig. 2 shows an example contact in one participant) in the upright and inverted conditions. Significant FID responses were determined by grouping the first four harmonics (i.e. summing 1.2, 2.4, 3.6 and 4.8 Hz, Fig. 2B) and computing a z-score transform ( $z > 3.1$ ,  $p < 0.001$ , Fig. 2C). In total, we found 295 contacts showing a significant FID response in either the upright or the inverted condition in 63 individual brains (among 3825 contacts implanted in the VOTC of 69 participants). When using a slightly less conservative threshold of  $z > 2.745$  ( $p < 0.003$ ) which was FDR-corrected (Benjamini and Hochberg, 1995) at  $p < 0.05$ , more FID contacts were identified but the pattern of results and data interpretation were extremely similar (Fig. S3).

The proportion of these FID contacts was significantly higher in the right (8.8%, 157/1794) than in the left hemisphere (6.8%, 138/2031,  $p = 0.02$ , 2-tailed permutation test). Among these 295 contacts, 161 were significant only in the upright condition, 75 only in the inverted condition, and 59 in both conditions (see examples in Figs. 2 and 3). For some of the analyses (i.e. proportion), FID contacts were further split in 2 sets based on the significance in the upright and inverted conditions: (1) UP contacts (i.e. showing a significant FID response in the upright



condition, regardless of the inverted condition, Fig. 3 left), and (2) INV contacts (i.e. showing a significant FID response in the inverted condition, regardless of the upright condition, Fig. 3 right). Some contacts exhibited significant responses in both upright and inverted conditions so that the 2 sets of contacts overlapped (Fig. 3 bottom; Fig. 4A).

Each significant FID contact was located and labeled according to the participant's individual anatomy (Table 1) using a topographic parcellation of the VOTC (Fig. S2; as in Jonas et al., 2016; Lochy et al., 2018). Moreover, to perform group visualization and analyses, the coordinates of each contact were transformed in the Talairach space (Fig. 4A). In the occipital lobe (OCC), FID responses were recorded in the inferior occipital gyrus (IOG) and in a large portion of the ventro-medial occipital cortex (VMO, Table 1, Fig. 4A). In the posterior temporal lobe (PTL), numerous FID responses were recorded in the lateral fusiform gyrus and adjacent occipito-temporal sulcus (latFG), as well as to a lesser extent in the medial fusiform gyrus and adjacent collateral sulcus (medFG), but very few in the lateral temporal cortex (inferior and middle temporal gyri, MTG/ITG). In the ATL (anterior to the posterior tip of the hippocampus, around Talairach y coordinate = -40, Fig. 4A), FID responses were observed in several distinct regions: along the anterior segments of the collateral sulcus (antCoS) and occipito-temporal sulcus (antOTS, located laterally to the CoS), in the anterior fusiform gyrus (antFG, located between the antCoS and the antOTS) and more laterally in the anterior part of the middle and inferior temporal gyri (antMTG/ITG). Finally, few FID responses were also found in the TP. Most of FID responses extended from approximately -100 to -5 along the antero-posterior Y axis in Talairach coordinates (Fig. 4A).

We investigated the spatial distribution of FID contacts separately for UP and INV contacts. Fig. 3 shows examples of these 2 contact types. There were 220 UP contacts and 134 INV contacts (59 contacts in common between the 2 orientations, see Fig. 3 bottom and Fig. 4A Venn diagram). Overall, the proportion of UP contacts (i.e. number of UP contacts divided by the number of recorded contacts) was significantly higher than INV contacts (UP = 220/3825 = 5.75% vs. INV = 134/3825 = 3.5%,  $p < 0.0001$ , 2-tailed permutation test). Both types of contacts were widely distributed across the VOTC (Fig. 4A).

### 3.2. Right VOTC shows higher proportion of UP FID contacts

To quantify and visualize the spatial distribution of UP and INV contacts at a more local level, we used Talairach transformed coordinates to compute the proportion of each type of contact (i.e. UP and INV) relative to the number recorded contacts in smaller volumes (i.e. 'voxels') (Fig. 4B, see also Fig. S4 for the left hemisphere lateral views). Computing such proportions allows taking into account the local variation in the number of recorded contacts across the VOTC. These proportion maps show that for both types of contacts, proportions significantly above zero ( $p < 0.01$ ) are found in the VMO and in the bilateral FG. For UP contacts, we also observed significant proportions in the ventral and lateral IOG, especially in the right hemisphere, and in more anterior portions of the bilateral temporal lobe (Fig. 4B, see the solid black contour lines on the left and middle maps). Statistically comparing proportion maps for UP vs. INV contacts reveals a significantly higher ( $p < 0.01$ ) proportion of UP contacts in the right hemisphere between approximately -80 mm to -10 mm along the postero-anterior axis of the Talairach space (i.e. y-dimension, Fig. 4B, right). More precisely, the significantly higher proportion of UP contacts started from the right IOG (mean Talairach antero-posterior y-coordinate of IOG contacts =  $-65 \pm 6$  mm) over ventral and lateral aspects (Fig. 4B, right), continuing anteriorly all along the right latFG (mean Talairach y-coordinate =  $-49 \pm 8$  mm), and up to the antFG ( $-25 \pm 7$  mm), antOTS ( $-28 \pm 10$  mm) and antCOS ( $-22 \pm 12$  mm). Notably, as depicted in Fig. 4B, this strip of cortex in the right hemisphere includes the mean peak coordinate of the FFA (in the latFG) as identified in fMRI in a meta-analysis (Berman et al., 2010, [39, -52, -15]), in a probabilistic atlas (Zhen et al., 2015, [38, -49, -18] converted from MNI to Talairach space), in a recent fMRI face lo-

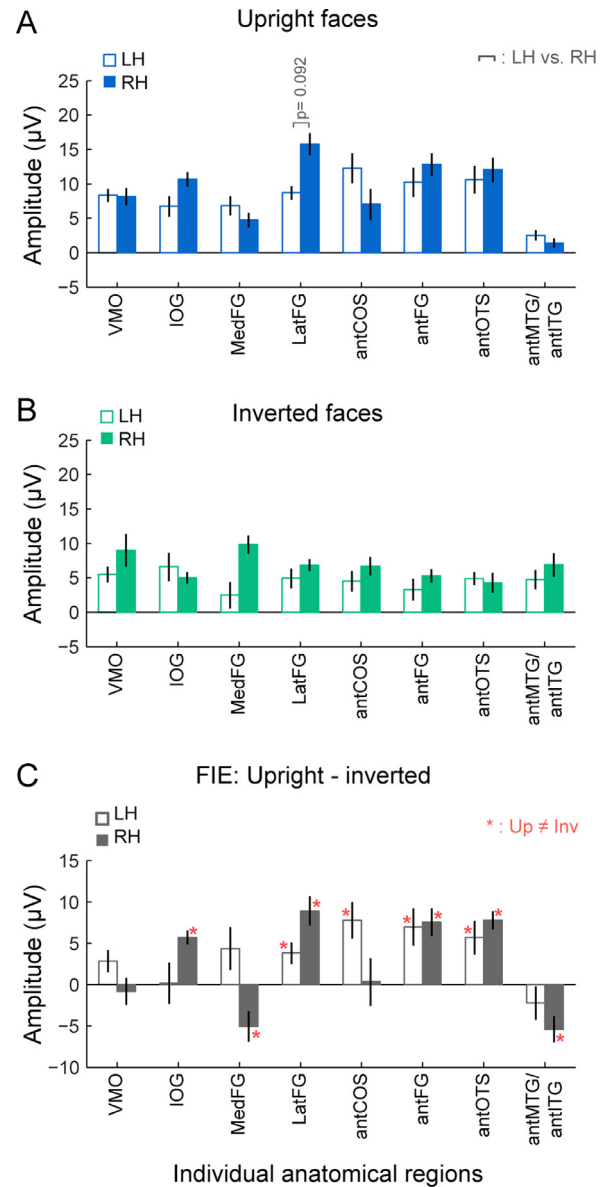


**Fig. 5.** Amplitude quantification in FID contacts. **A.** FID response amplitudes in the upright face condition over all FID contacts ( $N = 295$ ), for each anatomical region (i.e. as defined in the individual native anatomy) and separately for the left and right hemispheres (LH and RH respectively). Amplitudes are quantified as the mean of the amplitudes across recording contacts within a given anatomical region. Error bars are standard error of the mean across contacts. **B.** Same convention as for panel A but displaying amplitudes in the inverted face condition for the same contacts (FID contacts,  $N = 295$ ). **C.** Face inversion effect. Amplitude difference between upright and inverted face conditions are computed in each FID contact and averaged by anatomical region and hemisphere. Asterisks in red indicate significant (FDR-corrected) amplitude difference between upright and inverted face conditions, computed separately for each region and hemisphere using linear mixed models. Note that the mean amplitudes of FID responses in the MTG/ITG and TP are not reported as there were too few contacts in these regions to obtain reliable measures. (For interpretation of the references to colour in this figure legend, the reader is referred to the web version of this article.)

calizer using a frequency-tagging procedure similar to the present study (Gao et al., 2018, [42, -54, -14]), as well as the mean coordinate of the face-selective responses in the latFG in a recent intracerebral recording study (Jonas et al., 2016, [41, -45, -16]). This strip of cortex also includes the mean coordinates of the OFA in the inferior occipital gyrus as reported in a review (Pitcher et al., 2011b, [39, -74, -10]) or in a probabilistic atlas (Zhen et al., 2015, [39, -73, -13] converted from MNI to Talairach space). In the left hemisphere, we also found a higher proportion of UP contacts in the ATL and in a small portion of the IOG. Interestingly, the proportion of significant UP and INV contacts did not differ in the VMO. To statistically establish interhemispheric differences in the local proportions of UP vs. INV contacts, we compared this difference in proportion (i.e. UP vs. INV contacts) in corresponding voxels across hemispheres, restricting the comparison to voxels showing a significant difference between UP and INV contacts. This revealed that the difference in proportion of UP vs. INV contacts was significantly higher in the right hemisphere in portions of the IOG and latFG (Fig. 4B right, see the dashed black contour lines on the ventral map). Note that the proportion analyses yield virtually the same results whether or not the 13 participants with a BFRT-c score below the normal range were included in the analyses (Fig. S5).

### 3.3. Right hemispheric predominance of upright FID response amplitudes

We also quantified response amplitudes of the significant FID contacts ( $N = 295$ ). Unlike in the proportion analysis, this was performed by measuring the response amplitude for the upright and inverted conditions over the whole set of FID contacts (i.e. no longer splitting in UP and INV contacts). To do so, we summed the baseline-subtracted amplitude over the first 4 harmonics of the face identity change frequency (i.e. 1.2, 2.4, 3.6 and 4.8 Hz) for each significant FID contact (see Methods for details). We then calculated the mean amplitudes across FID contacts in each anatomical region, separately for the upright and inverted conditions (Fig. 5) and compared amplitudes across hemisphere using linear mixed model statistics. Note that the mean amplitudes of FID responses in the MTG/ITG and TP are not reported as there were too few contacts in these regions to obtain reliable measures (Table 1). In the upright condition (Fig. 5A), the largest FID response was recorded in the right latFG, followed by the right antFG, the left antCOS, the right antOTS and the right IOG. Only the latFG showed a trend for significant hemispheric difference ( $p = 0.09$ , FDR corrected,  $p = 0.01$  uncorrected), despite a large difference in the amplitude between left and right hemispheres for this region (Fig. 5A; the amplitude in the left latFG was 45% smaller than in the right latFG; computed as  $100 \cdot (R-L) / R$ ). When combining the two regions in the posterior temporal lobe with the highest proportions of FID contacts (i.e. the latFG and IOG), the amplitude in the right hemisphere was significantly higher than in the left hemisphere ( $13.22 \mu\text{V}$  vs.  $8.04 \mu\text{V}$ ,  $p = 0.021$ ). In the inverted face condition, the overall amplitudes across the VOTC were reduced compared to the upright condition (Fig. 5B) and the largest responses were found in the right medFG, followed by the right VMO. No significant interhemispheric differences were found in the inverted face condition.

Next, we quantified the face inversion effect in each region by subtracting the response amplitude in inverted condition from the response in the upright condition for each contact and then averaging across contacts (Fig. 5C). FID responses were significantly higher in the upright compared to inverted conditions in several regions: the right IOG (mean amplitude difference between upright and inverted  $\pm$  S.D. =  $5.7 \mu\text{V} \pm 4.8$ ,  $p < 0.0001$ , FDR-corrected, Fig. 5C; percentage of amplitude reduction for INV vs. UP =  $-53\%$ , computed as  $100 \cdot (\text{UP} - \text{INV}) / \text{UP}$ ), the left and right latFG (respectively  $3.8 \mu\text{V} \pm 6.1$ ,  $p < 0.005$  and  $8.9 \mu\text{V} \pm 10.1$ ,  $p < 0.0002$ , i.e.  $-44\%$  and  $-56\%$  of reduction for inverted faces), the left and right antFG ( $7.5 \mu\text{V} \pm 6.5$ ,  $p < 0.05$  and  $6.9 \mu\text{V} \pm 5.5$ ,  $p < 0.0005$ ;  $-68\%$  and  $-59\%$  of reduction for inverted faces), the left antCOS ( $3.8 \mu\text{V} \pm 6.1$ ,  $p < 0.01$ ;  $-63\%$ ), and the left and right antOTS ( $5.7 \mu\text{V} \pm 9.8$ ,  $p < 0.01$  and  $7.8 \mu\text{V} \pm 3.5$ ,  $p < 0.0005$ ;  $-54\%$  and  $-65\%$  respec-

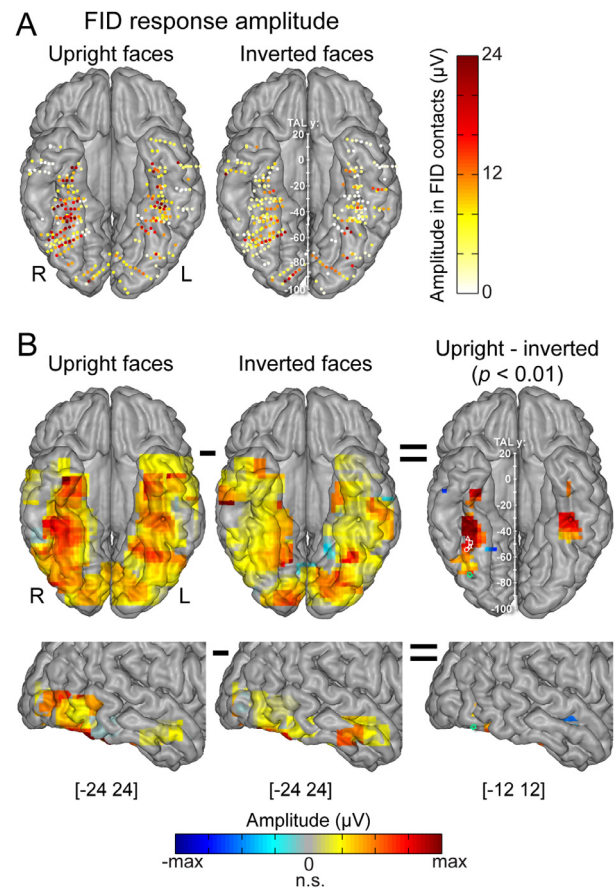


**Fig. 6.** Spatial distribution and response amplitude over FID contacts in the Talairach space. **A.** Map of all FID contacts ( $N = 295$ ) across 69 individual brains displayed in the Talairach space. Each circle represents a single contact color-coded according to its FID response amplitude in the upright face (left) or inverted face (right) condition. For visualization purposes, individual contacts are displayed larger than their actual size (2 mm in length). **B.** Ventral and right lateral maps showing smoothed response amplitude over FID contacts displayed over the VOTC cortical surface for the upright face (left) and inverted face (middle) conditions, and maps of the significant amplitude difference ( $p < 0.01$ ) between upright and inverted face conditions (right). The coordinates of published peak location of face-selective regions are shown in white for fMRI-defined FFA (star: Berman et al., 2010, circle: Gao et al., 2018, square: Zhen et al., 2015), in green for fMRI-defined OFA (square: Zhen et al., 2015, diamond: Pitcher et al., 2011b) and the mean coordinates for latFG face-selective responses in a recent SEEG study are displayed with a white triangle (Jonas et al., 2016). (For interpretation of the references to colour in this figure legend, the reader is referred to the web version of this article.)

tively). We also found the opposite pattern with significantly larger FID responses for inverted compared to upright faces in the right medFG ( $-5.1 \mu\text{V} \pm 7.4$ ,  $p < 0.01$ ,  $+108\%$ ) and right antMTG/ITG ( $-5.4 \mu\text{V} \pm 5.7$ ,  $p = 0.0015$ ,  $+384\%$ ). The face inversion effect measured in the IOG and latFG was larger in the right compared to left hemisphere (65% smaller in the left hemisphere when combining the two regions). However, owing to the high variability of amplitude values across patients ( $n = 13$  and  $n = 12$  for left and right hemisphere, respectively) in these regions, this difference did not reach significance.

As in the proportion analyses above, we also examined the distribution of response amplitudes without a priori regional grouping by generating VOTC maps of the amplitudes of all FID contacts ( $N = 295$ ) in the Talairach space. FID amplitudes were displayed either at the level of each individual contact (Fig. 6A) or averaged within voxels projected to the cortical surface (Fig. 6B, see also Fig. S4 for the left hemisphere lateral views). As expected from the previously described regional aver-

ages, the highest response amplitude was located in the right latFG in the upright condition. A statistical comparison of upright and inverted amplitude maps revealed significantly higher responses for upright faces predominantly in the right hemisphere, stretching along the postero-anterior axis starting from the right IOG, to the right latFG, and up to the ATL region (Fig. 6B, right). Similarly to the significantly higher proportion of UP contacts in the right hemisphere (Fig. 4B, right), this face inversion effect amplitude difference also extended from approximately  $-75$  mm to  $-7$  mm on the antero-posterior Y axis of the Talairach space. This strip of cortex in the right hemisphere showing a face inversion effect in amplitude includes the mean peak coordinate of the FFA (Berman et al., 2010; Gao et al., 2018; Zhen et al., 2015), the mean coordinate of the face-selective responses in the latFG in a recent SEEG study (Jonas et al., 2016) and the mean coordinates of the OFA (Pitcher et al., 2011b; Zhen et al., 2015) (Fig. 6B, right). We also found significantly higher amplitudes in the upright condition in the left hemisphere, restricted to the anterior portion of the latFG and posterior portions of the antCOS, antFG and antOTS (Fig. 6B and 5C). Interestingly, while there were clear responses over the posterior VOTC (VMO), these responses were of similar magnitude in the upright and inverted conditions, as indicated by an absence of significant difference across conditions in this region (Fig. 6B, see also Fig. 5C). As for the proportion analyses, note that the amplitude analyses yield virtually the same results whether or not the 13 participants with a BFRT-c score below the normal range were included in the analyses (Fig. S5 and Fig. S6).

Last, we further investigated whether the neural processes involved in generating FID responses in the upright and inverted conditions were qualitatively different by correlating the response amplitude in the two conditions across regions ( $N = 18$  across the 2 hemispheres) and FID contacts ( $N = 295$ ). The resulting correlations were weak: Pearson  $r = -0.18$  ( $p = 0.47$ , randomization test where the null distribution is generated by randomly shuffling the pairing of amplitudes) and  $0.14$  ( $p < 0.0063$ ), respectively for correlations using regions or contacts. Although the correlation using all FID contacts was significantly different from zero, it has very low explanatory power, accounting for only 2% of shared variance.

#### 4. Discussion

We report an original neural cartography of unfamiliar face individuation across the human VOTC, using data collected in a large sample of individuals implanted with intracerebral electrodes. To our knowledge, only a handful of studies reported human intracranial recordings during unfamiliar FID. Specifically, Puce et al. (1999) showed amplitude decreases of low-frequency late ECoG (Electrocorticography) responses in the ATL to repeated presentations of faces, while Engell and McCarthy (2014) described high-frequency activity decreases over the middle FG at an earlier latency with a subset of the same data. Using MVPA, Ghuman et al. (2014) found significant decoding of individual face images and features in 4 patients with recordings over the middle FG, and Davidesco et al. (2014) were able to decode 14 different images of faces in the posterior ventral and lateral occipito-temporal cortex using data recorded in 14 patients with both ECoG and SEEG.

While the current observations generally agree with these previous findings, the present investigation goes well beyond these studies by mapping neurophysiological FID responses across the whole human VOTC, sampling both gyri and sulci thanks to the SEEG approach, in a large number of individual brains (Rossion et al., 2018). Importantly, the strengths of the current FPVS paradigm enable to capture neural responses directly reflecting visual face identity processing. Hence, not only does this paradigm have high validity, objectivity, sensitivity, and reliability, but it also offers control for individuation based on low-level features through the speed and large number of variable individual discriminations occurring during a sequence, the requirement to generalize across stimulus size (Dzhelyova and Rossion, 2014; Liu-Shuang et al., 2014), and most importantly, through the comparison to

the exact same stimulation with faces presented in the inverted orientation (Rossion et al., 2020).

Our comprehensive intracerebral mapping of the VOTC reveals four key findings characterizing the FID function in the human brain. First, we find a robust face inversion effect as demonstrated by a larger proportion of significant contacts and higher FID response amplitudes for upright than inverted faces. Second, the face inversion effect is spatially distributed yet confined to a relatively narrow strip of cortex extending from the right posterior VOTC (IOG and latFG) to bilateral ATL regions. Third, our study identifies clear FID responses in the anterior FG and surrounding sulci, up to 3 cm more anterior than the latFG. Fourth, almost no FID responses are found in very anterior ATL regions, including the temporal pole, despite extensive sampling of this region.

##### 4.1. The effect of stimulus inversion on face individuation

Picture-plane inversion dramatically affects behavioral individuation of faces in humans (Rossion, 2008; Yin, 1969), therefore allowing to isolate high-level neural processes subtending FID, i.e. processes that go beyond the discrimination of physical differences between face images (which are strictly identical regardless of orientation). Interestingly, our extensive spatial sampling reveals substantial differences across brain regions in terms of the FID response amplitude and the proportion of significant contacts for upright and inverted faces. On recording contacts located closely to or in low-level visual cortical regions ("VMO"), there was little to no difference between FID responses to upright and inverted faces, suggesting that the small effects found in these regions are based on low-level visual cues. In contrast, multiple higher-order cortical regions, i.e., in the posterior and anterior ventral temporal cortex, showed a robust reduction of amplitude and proportion of significant contacts for inverted compared to upright faces. These findings directly contradict the view that unfamiliar faces are individuated by low-level visual processes/cues in the human brain similarly for upright and inverted faces (Hancock et al., 2000; Megreya & Burton, 2006; Burton, 2013). Moreover, according to a quantitative view of the face inversion effect (e.g., Murphy et al., 2020; Sekuler et al., 2004), the decrease of amplitude for inverted faces should be uniformly observed, and proportional across brain regions (i.e., no interaction between inversion and cortical localization). Instead, the large differences in the face inversion effect observed between regions as described above, as well as the null or very weak correlation between FID amplitude for upright and inverted faces across electrode contacts, rather fully support a qualitative view of this effect (Rossion, 2008).

The reduction of amplitude for inverted faces was most prominent in the right hemisphere, where it ranged from 53% (IOG) to 65% (antOTS). Intriguingly, the magnitude of the face inversion effect observed in the right IOG and latFG ( $-53\%$  and  $-56\%$  respectively) is in striking correspondence with scalp EEG results over the right hemisphere in neurotypical adult participants, showing a 53% decrease in FID response amplitude with inversion (Rossion et al., 2020). The location of this effect is also largely in line with fMRI-adaptation studies reporting significantly larger repetition suppression for upright than inverted faces in well-defined bilateral face-selective regions of the latFG (i.e., the FFA) and, to a lesser extent, of the IOG (OFA; Gilaie-Dotan et al., 2010; Mazard et al., 2006; Yovel and Kanwisher, 2005). The role of the right IOG in FID has sometimes been related to the processing of low-level facial features due to the lack of a behavioral inversion effect when stimulating this region with transcranial magnetic stimulation (TMS) (Pitcher et al., 2011a). In contrast with this view, our data unambiguously shows a robust and right lateralized effect of inversion on FID in this region.

Inversion also largely modulated FID responses in the ATL (antCOS, antFG, and antOTS), reaching up to  $-65\%$  in the right antOTS. To our knowledge, such effects have not been reported, most likely owing to the large signal drop-out in these ventral ATL regions in fMRI (Axelrod and Yovel, 2013; Rossion et al., 2018; Wandell, 2011). In ad-

dition, there was no inversion effect in more medial regions (medFG) or more lateral regions of the VOTC (MTG/ITG, antMTG/ITG), with the right medFG even exhibiting the opposite pattern of larger FID responses to inverted than to upright faces. Larger responses to inverted compared to upright faces (regardless of identity) have been observed previously in fMRI over medial regions of the VOTC such as the parahippocampal gyrus or medial fusiform gyrus (Aguirre et al., 1999; Gilaie-Dotan et al., 2010; Haxby et al., 1999; Rosenthal et al., 2016), with one study reporting larger repetition suppression effects for inverted than for upright individual unfamiliar faces in the parahippocampal gyrus (Gilaie-Dotan et al., 2010). Since these regions typically show reduced responses to faces relative to visual objects in fMRI (Aguirre et al., 1999; Haxby et al., 1999), these effects have been interpreted in terms of the recruitment of processing resources from object perception systems for inverted faces (see also Rosenthal et al., 2016). Our findings with direct recordings of neural activity in VOTC support these observations.

#### 4.2. A confined distribution of cortical face individuation responses in the right hemisphere

While individuation of inverted faces is not necessarily based on low-level visual cues, comparing upright and inverted faces nevertheless allows to isolate high-level processes, i.e. going beyond physical differences between stimuli. Hence, in the remaining of the discussion, we focus on the differential FID maps for this comparison. The large-scale proportion and the amplitude maps (Figs. 4 and 6), which largely agree with each other, indicate that unfamiliar FID in humans is not limited to a local brain region but is instead achieved by widely distributed populations of neurons. Specifically, high-level unfamiliar FID is supported by a strip of cortex in the right VOTC including the right IOG, the right latFG and the right ATL region just anterior to the latFG (antCOS, antFG and antOTS), as well as the latter region in the left hemisphere. Face-selective activations typically identified in fMRI studies in the IOG (OFA, Gauthier et al., 2000; Pitcher et al., 2011b; Zhen et al., 2015) and latFG (FFA, Berman et al., 2010; Gao et al., 2018; Kanwisher et al., 1997; Zhen et al., 2015; pFUS and mFUS, Weiner and Grill-Spector, 2012; see also Jonas et al., 2016 for latFG face-selective responses in SEEG) fall within this strip of cortex (Figs. 4B and 6B). This is supported by the similarity both in terms of the anatomical location in individual brains in the current study and in terms of mean Talairach coordinates. As mentioned earlier, these two functional regions are known to be involved in FID, based on fMRI-adaptation effects. However, although these effects are often found bilaterally in these regions (see Rossion, 2014 for review), lesion studies, as well as effects of transcranial and intracranial stimulation on FID clearly point to a right hemisphere dominance of these regions (Bouvier and Engel, 2006; Jonas et al., 2018, 2014; Meadows, 1974; Pitcher et al., 2007). Such right hemispheric dominance is clearly supported by the present direct recordings of intracerebral neurophysiological responses, in line with effects observed on the scalp in the same paradigm (Liu-Shuang et al., 2014; Rossion et al., 2020). The lack of strong right hemispheric lateralization of this effect in fMRI may be due to the slow temporal dynamics of the fMRI responses, which favors a spread of responses to the other hemisphere.

Importantly, despite their wide cortical distribution, high-level unfamiliar FID responses are not found everywhere in the occipito-temporal cortex. Rather, they are anatomically confined to the right IOG, the right latFG and extending to the bilateral ATL. Whether this cortical strip appears continuous due to the averaging methods across individual brains or reflects a genuine functional organization cannot be determined with the present dataset. Again, fMRI-adaptation studies have investigated the sensitivity to individual face identities within focal face-selective regions of the IOG and latFG spatially segregated in each participant's brain (e.g., Eger et al., 2004; Ewbank et al., 2013; Gauthier et al., 2000; Hermann et al., 2017; Hughes et al., 2019; Rostalski et al., 2019; Schiltz and Rossion, 2006). The variable localizations of these fMRI regions-of-interest across individual brains coupled with a superimpo-

sition of neural activity across brains as performed here could result in a visually artificial continuous strip subtending the FID function. Alternatively, fMRI studies may only identify the tip(s) of the iceberg(s), i.e. local regions with the highest density of neurons sensitive to face identity, these neurons being nevertheless distributed continuously all along the IOG, latFG and the ATL. In other words, the FID function may well be truly continuously distributed along the (right) IOG, latFG and ATL, with local clusters of neuronal populations being most critical for the function. Supporting this latter point, rare transient behavioral disruptions of FID due to intracerebral electrical stimulation appears to be confined to regions showing the largest face-selective and FID responses (Jonas et al., 2018, 2014).

#### 4.3. The role of the anterior fusiform gyrus and surrounding sulci in FID

Our investigation identified regions anterior to the latFG/FFA as being involved in unfamiliar FID. Hence, the cortical maps showed that FID responses extended anteriorly and bilaterally in the ATL, up to about 3 cm beyond the anterior part of the latFG (i.e. starting at Talairach y coordinate around  $-40$ ) but not covering the most anterior part of the ATL (i.e. anterior to around  $y = -7$  Talairach coordinate; see the discussion below). This region corresponds anatomically to the anterior fusiform gyrus and its 2 adjacent sulci, antCOS and antOTS (for simplicity, we will refer to this region as antFG+sulci). The effects of inversion are particularly large (i.e., 65%) in this antFG+sulci region, except in the right antCOS. While FID is strictly right lateralized in the posterior temporal lobe (IOG and latFG), FID is found bilaterally in the antFG+sulci, pointing to a functional difference from posterior FID regions.

Since the antFG+sulci is located at the heart of the largest VOTC magnetic susceptibility artifact in fMRI (e.g., Axelrod and Yovel, 2013; Jonas et al., 2015; Rossion et al., 2018; Wandell, 2011), its contribution to FID and face processing in general has been largely unexplored. In fact, this region lies more anteriorly than the reported location of the most anterior face-selective activation in the latFG measured with fMRI (FFA1 / mFus; Pinsk et al., 2009; Weiner et al., 2014). It is also more anterior and lateral than the antFG region showing above chance decoding of individual faces as reported in a MVPA-fMRI study (Nestor et al., 2016). However, the antFG+sulci region has been singled out as showing categorical differences between unfamiliar and familiar faces during an orthogonal task in an early Positron Emission Tomography study (Rossion et al., 2001) and has been associated with reduced cortical volume in low performers at face identity recognition (Behrmann et al., 2007). Intracerebral electrical stimulation of this region in the right hemisphere can also lead to temporary selective familiar face identity recognition impairments (Jonas et al., 2015). The present findings suggest that this transient interruption could be due to a failure to individuate faces based on visual representations rather than access to specific semantic information about people.

#### 4.4. Lack of temporal pole FID responses: an effect of unfamiliarity?

Despite extensive sampling of the ATL up to the temporal pole, FID responses are weak and rare in the most anterior part of the ATL (anterior to around  $-7$  Talairach y coordinate) and in the temporal pole (except in the left hemisphere in the proportion map). Over the last decade, ATL regions, in particular in the temporal pole, have been attributed a prominent role in face processing (Avidan et al., 2014; Axelrod and Yovel, 2013; Rajimehr et al., 2009; Von Der Heide et al., 2013). Some studies, relying primarily on fMRI-MVPA reports of above chance unfamiliar face identity decoding in this region, have even claimed it as a primary locus of face identity recognition (Anzellotti et al., 2014; Kriegeskorte et al., 2007). However, the localization of decoding effects is inconsistent across these studies, these effects are usually just above chance level and may not be specific to identity (e.g., decoding between a single male and female face picture in Kriegeskorte et al., 2007). Most importantly, cortical damage to this region is not typically

associated with prosopagnosia – an impairment of face identity recognition limited to the visual modality – but rather with multimodal semantic memory impairments, as in the right hemispheric fronto-temporal variant of semantic dementia (Busigny et al., 2009; Evans et al., 1995; Gainotti et al., 2008; Lambon Ralph, 2014). Together with the present findings based on an extensive spatial sampling of the FID function in the ATL, this suggests that the temporal pole is not critical for visual face identity recognition. Instead, this region may be involved in the association of semantic information with specific face identities, including verbal labels (Collins et al., 2016; Rice et al., 2018; Von Der Heide et al., 2013). If this reasoning is correct, the same frequency-tagging approach as used here but with pictures of familiar(ized) faces (Verosky et al., 2020) should reveal an increased contribution of ATL regions including the temporal poles.

#### 4.5. Potential limitations and future extensions

Although we isolated high-level visual responses supporting FID by comparing upright and inverted faces, the present frequency-tagging paradigm is based on the repetition of the exact same image (at different sizes) of a full-front face identity, interrupted periodically by other facial identities also presented at a full-front view. Hence, we did not evaluate FID responses across natural changes of viewing conditions, e.g. in head rotation and lighting direction (O'Toole et al., 2006; Rossion and Michel, 2018; Tarr and Bülthoff, 1998). Scalp EEG data collected with this paradigm show that the FID response to unfamiliar faces remains robust through random variations in head pose (e.g., head tilted down, looking upward, to the side, etc.) throughout the stimulation sequence (Damon et al., 2020). The FID response is also strong when head orientation varies randomly in depth (i.e. full-front faces, profile,  $\frac{3}{4}$  profile faces, etc.) but decreases linearly over the right occipito-temporal cortex with increasing viewpoint variation (Rossion et al., 2020), indicating that this response is viewpoint-dependent to some extent. Exploring the neural basis of this viewpoint-dependency with the present intracerebral recording approach would be highly valuable, in particular to evaluate whether there is a progressive increase of invariance to changes in viewing conditions in FID responses from posterior (IOG) to more anterior (latFG or antFG) regions in the human brain (see Ramirez, 2018).

An important issue to consider is that the data reported here was collected on a specific clinical population, namely patients with long-term drug-resistant epilepsy. Most participants tested here have temporal lobe epilepsy which may cause (visual) recognition deficits. Neuropsychological studies have shown that this population, on average, suffers from increased difficulties at encoding and recognizing familiar faces (Drane et al., 2013). However, there is also a wide interindividual variability in this function in the normal population (Jenkins et al., 2018), and there is currently no evidence that these face identity encoding and recognition processes are qualitatively different in temporal lobe epilepsy patients than in the normal population. Moreover, to our knowledge, there is no evidence that temporal lobe epilepsy patients have difficulties to individuate *unfamiliar faces* (Chiaravalloti and Glosser, 2004). A subset of 32 participants of our sample performed a behavioral delayed face matching task (experiment 4 of Busigny and Rossion, 2010) and showed large, normal range, face inversion effects both in accuracy rates and response times (Fig. S1). Also, most of our participants (84%) were tested at the Benton Face Recognition Test-c (Rossion and Michel, 2018), reaching an average performance in the normal range. While 13 participants showed a score below normal range (<39), the outcome of the proportion and amplitude analyses reported here was not affected by the inclusion of these participants (Fig. S5 and S6). This supports the view that lower performance (and higher reaction times) at explicit behavioral tasks of face individuation in some of these temporal lobe epilepsy patients are not due to specific face individuation deficits. Instead, these difficulties may be due to lower levels of education and general cognitive impairments (see Benton et al., 1983;

Schretlen et al., 2001 for BFRT performance; see also Fig. S1 for performance at the face matching task in the present sample).

Another related issue is that of the potential neuro-functional reorganization of face processing in this population of temporal lobe epilepsy patients. Here, contrary to weakly substantiated claims of such reorganization (Mogi et al., 2019; Riley et al., 2015), our observations of large neural face inversion effects, right hemispheric lateralization and confined localization of FID responses in the IOG and latFG in our sample of patients are in general agreement with multiple sources of evidence from lesion studies, neuroimaging and effects of intracerebral or transcranial stimulation as reviewed in the introduction. In addition, there is a close correspondence between the present findings from temporal lobe epilepsy patients in SEEG and normal controls tested with the exact same experimental paradigm in scalp EEG. Specifically, the magnitude of the face inversion effect in the two key regions of the right IOG and latFG (53% and 56% reduction respectively) is strikingly similar to the effect found on the scalp over the right occipito-temporal region (53% reduction; Rossion et al., 2020). As for the right hemispheric lateralization index, it is at least as large in these two regions here (37% and 45% right IOG and latFG respectively) as it is on the scalp in neurotypical individuals (27%; Rossion et al., 2020). These observations do not only strengthen the validity of the present findings, but also neurophysiological data recordings in temporal lobe epilepsy patients to understand human face recognition and brain function in general.

A future extension of this study would be to determine *when* and *how* unfamiliar FID is achieved in the human brain. Answering the question of the time-course of FID could be potentially addressed by analyzing the present data in the time-domain (Rossion et al., 2020). However, unlike the frequency-domain approach used here, which provides an objective compact measure of the function, the temporal decomposition of the response yields numerous deflections over time (Dzhelyova and Rossion, 2014; Rossion et al., 2020). Inside the brain, these local field potentials occur with opposite polarities in interlocked time-courses depending on the recording sites and reference electrode (e.g., Barbeau et al., 2008), making it extremely challenging to combine participants to obtain an intelligible representation across the whole neural circuitry. Determining *how* (i.e., neural mechanisms) unfamiliar FID is achieved in the human brain would require recording at lower-levels of neural organization to capture the activity of single units in humans (Quiñones Quiroga, 2012; Rey et al., 2020). Importantly, the findings of the present study indicate that the neuronal code for human face individuation is unlikely to be cracked by focusing on small local populations of neurons but will rather require recordings at multiple VOTC locations, preferentially in the right hemisphere.

## 5. Summary and conclusions

In summary, our large scale human intracerebral investigation shows that fast, automatic and high-level unfamiliar face individuation in humans is achieved by neural populations distributed within a strip of cortex running from the IOG and latFG to the antFG and surrounding sulci, with a right hemispheric dominance. These observations fully support the qualitative view of the face inversion effect. They also highlight the importance of probing the neural basis of human FID with unfamiliar faces in order to isolate visual processes subtending this function from the contribution of associated semantic, affective and verbal information.

### CRedit authorship contribution statement

**Corentin Jacques:** Conceptualization, Methodology, Software, Formal analysis, Visualization, Writing - original draft, Writing - review & editing. **Bruno Rossion:** Conceptualization, Methodology, Project administration, Writing - original draft, Supervision, Funding acquisition, Writing - review & editing. **Angélique Volfart:** Investigation, Formal

analysis, Visualization. **Hélène Brissart**: Investigation, Formal analysis. **Sophie Colnat-Coulbois**: Resources, Investigation. **Louis Maillard**: Resources, Project administration, Funding acquisition. **Jacques Jonas**: Conceptualization, Methodology, Investigation, Resources, Visualization, Writing - original draft, Writing - review & editing.

## Acknowledgments

We thank the participants for their involvement in the study. We thank Joan Liu-Shuang for her contribution to the research design and EEG data collection. This work is supported by an EOS grant “HUMVIS-CAT” 30991544.

## Supplementary materials

Supplementary material associated with this article can be found, in the online version, at doi:10.1016/j.neuroimage.2020.117174.

## References

- Aguirre, G.K., Singh, R., D'Esposito, M., 1999. Stimulus inversion and the responses of face and object-sensitive cortical areas. *Neuroreport* 10, 189–194.
- Anzellotti, S., Fairhall, S.L., Caramazza, A., 2014. Decoding representations of face identity that are tolerant to rotation. *Cereb. Cortex* 24, 1988–1995. doi:10.1093/cercor/bht046.
- Avidan, G., Tanzer, M., Hadj-Bouziane, F., Liu, N., Ungerleider, L.G., Behrmann, M., 2014. Selective dissociation between core and extended regions of the face processing network in congenital prosopagnosia. *Cereb. Cortex* 24, 1565–1578. doi:10.1093/cercor/bht007.
- Axelrod, V., Vovel, G., 2013. The challenge of localizing the anterior temporal face area: a possible solution. *Neuroimage* 81, 371–380. doi:10.1016/j.neuroimage.2013.05.015.
- Barbeau, E.J., Taylor, M.J., Regis, J., Marquis, P., Chauvel, P., Liégeois-Chauvel, C., 2008. Spatio-temporal dynamics of face recognition. *Cereb. Cortex* 18, 997–1009. doi:10.1093/cercor/bhm140.
- Barton, J.J.S., 2008. Structure and function in acquired prosopagnosia: lessons from a series of 10 patients with brain damage. *J. Neuropsychol.* 2, 197–225. doi:10.1348/174866407x214172.
- Bates, D., Mächler, M., Bolker, B., Walker, S., 2015. Fitting Linear Mixed-Effects Models Using lme4. *J. Stat. Softw.* 67, 1–48. doi:10.18637/jss.v067.i01.
- Baylis, G.C., Rolls, E.T., Leonard, C.M., 1985. Selectivity between faces in the responses of a population of neurons in the cortex in the superior temporal sulcus of the monkey. *Brain Res* 342, 91–102.
- Behrmann, M., Avidan, G., Gao, F., Black, S., 2007. Structural imaging reveals anatomical alterations in inferotemporal cortex in congenital prosopagnosia. *Cereb. Cortex* 17, 2354–2363. doi:10.1093/cercor/bhl144.
- Benjamini, Y., Hochberg, Y., 1995. Controlling the false discovery rate: a practical and powerful approach to multiple testing. *J. R. Stat. Soc. Ser. B* 57, 289–300.
- Benton, A.L., Sivan, A.B., Hammers, K., Varney, N.R., Spreen, O., 1983. *Contributions to Neuropsychological Assessment: A Clinical Manual*, Oxford Uni. Oxford University Press, New York ed.
- Benton, A.L., Van Allen, M.W., 1968. Impairment in facial recognition in patients with cerebral disease. *Trans. Am. Neurol. Assoc.* 93, 38–42.
- Berman, M.G., Park, J., Gonzalez, R., Polk, T.A., Gehrke, A., Knaffla, S., Jonides, J., 2010. Evaluating functional localizers: the case of the FFA. *Neuroimage* 50, 56–71. doi:10.1016/j.neuroimage.2009.12.024.
- Bodamer, J., 1947. Die-Prosop-agnosie. *Arch. Psychiatr. Nervenkrankh* 179, 6–54.
- Bouvier, S.E., Engel, S.A., 2006. Behavioral deficits and cortical damage loci in cerebral achromatopsia. *Cereb. Cortex* 16, 183–191.
- Bruce, C., 1982. Face recognition by monkeys: absence of an inversion effect. *Neuropsychologia* 20, 515–521. doi:10.1016/0028-3932(82)90025-2.
- Busigny, T., Robaye, L., Dricot, L., Rossion, B., 2009. Right anterior temporal lobe atrophy and person-based semantic deficit: a detailed case study. *Neurocase* 15, 485–508. doi:10.1080/13554790902971141.
- Burton, M., 2013. Why has research in face recognition progressed so slowly? The importance of variability. *Q. J. Exp. Psychol.* 66, 1467–1485. doi:10.1080/17470218.2013.800125.
- Busigny, T., Rossion, B., 2010. Acquired prosopagnosia abolishes the face inversion effect. *Cortex* 46, 965–981. doi:10.1016/j.cortex.2009.07.004.
- Carey, S., 1992. Becoming a face expert. *Philos. Trans. R. Soc. Lond. B. Biol. Sci.* 335, 93–95. doi:10.1098/rstb.1992.0012.
- Chang, L., Tsao, D.Y., 2017. The code for facial identity in the primate brain. *Cell* 169, 1013–1028. doi:10.1016/j.cell.2017.05.011.
- Chiaravalloti, N.D., Glosser, G., 2004. Memory for faces dissociates from memory for location following anterior temporal lobectomy. *Brain Cogn* 54, 35–42. doi:10.1016/s0278-2626(03)00257-4.
- Collins, J.A., Koski, J.E., Olson, I.R., 2016. More than meets the eye: the merging of perceptual and conceptual knowledge in the anterior temporal face area. *Front. Hum. Neurosci.* 10, 189. doi:10.3389/fnhum.2016.00189.
- Cox, R.W., 1996. AFNI: software for analysis and visualization of functional magnetic resonance neuroimages. *Comput. Biomed. Res.* 29, 162–173. doi:10.1006/cbmr.1996.0014.
- Damon, F., Leleu, A., Rekow, D., Poncet, F., Baudouin, J.Y., 2020. Expertise for conspecific face individuation in the human brain. *Neuroimage* 204, 116218. doi:10.1016/j.neuroimage.2019.116218.
- Davidesco, I., Zion-Golumbic, E., Bickel, S., Harel, M., Groppe, D.M., Keller, C.J., Schevon, C.A., McKhann, G.M., Goodman, R.R., Goelman, G., Schroeder, C.E., Mehta, A.D., Malach, R., 2014. Exemplar selectivity reflects perceptual similarities in the human fusiform cortex. *Cereb. Cortex* 24, 1879–1893. doi:10.1093/cercor/bht038.
- Drane, D.L., Ojemann, J.G., Phatak, V., Loring, D.W., Gross, R.E., Hebb, A.O., Silbergeld, D.L., Miller, J.W., Voets, N.L., Saindane, A.M., Barsalou, L., Meador, K.J., Ojemann, G.A., Tranel, D., 2013. Famous face identification in temporal lobe epilepsy: support for a multimodal integration model of semantic memory. *Cortex* 49, 1648–1667. doi:10.1016/j.cortex.2012.08.009.
- Dzhelyova, M., Jacques, C., Dormal, G., Michel, C., Schiltz, C., Rossion, B., 2019. High test-retest reliability of a neural index of rapid automatic discrimination of unfamiliar individual faces. *Vis. Cogn.* 27, 127–141. doi:10.1080/13506285.2019.1616639.
- Dzhelyova, M., Rossion, B., 2014. The effect of parametric stimulus size variation on individual face discrimination indexed by fast periodic visual stimulation. *BMC Neurosci* 15, 87. doi:10.1186/1471-2202-15-87.
- Eger, E., Schyns, P.G., Kleinschmidt, A., 2004. Scale invariant adaptation in fusiform face-responsive regions. *Neuroimage* 22, 232–242.
- Engell, A.D., McCarthy, G., 2014. Repetition suppression of face-selective evoked and induced EEG recorded from human cortex. *Hum. Brain Mapp.* 35, 4155–4162. doi:10.1002/hbm.22467.
- Evans, J.J., Heggs, A.J., Antoun, N., Hodges, J.R., 1995. Progressive prosopagnosia associated with selective right temporal lobe atrophy. A new syndrome? *Brain* 118, 1–13. doi:10.1093/brain/118.1.1, Pt 1.
- Ewbank, M.P., Henson, R.N., Rowe, J.B., Stoyanova, R.S., Calder, A.J., 2013. Different neural mechanisms within occipitotemporal cortex underlie repetition suppression across same and different-size faces. *Cereb. Cortex* 23, 1073–1084. doi:10.1093/cercor/bhs070.
- Farah, M.J., 1990. *Visual agnosia: disorders of object recognition and what they tell us about normal vision.*, *Visual agnosia: disorders of object recognition and what they tell us about normal vision. Issues in the Biology of Language and Cognition.* The MIT Press, Cambridge, MA, US.
- Gainotti, G., Ferraccioli, M., Quaranta, D., Marra, C., 2008. Cross-modal recognition disorders for persons and other unique entities in a patient with right fronto-temporal degeneration. *Cortex* 44, 238–248. doi:10.1016/j.cortex.2006.09.001.
- Gao, X., Gentile, F., Rossion, B., 2018. Fast periodic stimulation (FPS): a highly effective approach in fMRI brain mapping. *Brain Struct. Funct.* doi:10.1007/s00429-018-1630-4.
- Gauthier, I., Tarr, M.J., Moylan, J., Skudlarski, P., Gore, J.C., Anderson, A.W., 2000. The fusiform “face area” is part of a network that processes faces at the individual level. *J. Cogn. Neurosci.* 12, 495–504. doi:10.1162/0899892900562165.
- Ghuman, A.S., Brunet, N.M., Li, Y., Konecky, R.O., Pyles, J.A., Walls, S.A., Destefno, V., Wang, W., Richardson, R.M., 2014. Dynamic encoding of face information in the human fusiform gyrus. *Nat. Commun.* 5, 1–10. doi:10.1038/ncomms6672.
- Gilade-Dotan, S., Gelbard-Sagiv, H., Malach, R., 2010. Perceptual shape sensitivity to upright and inverted faces is reflected in neuronal adaptation. *Neuroimage* 50, 383–395. doi:10.1016/j.neuroimage.2009.12.077.
- Goesaert, E., Op de Beeck, H.P., 2013. Representations of facial identity information in the ventral visual stream investigated with multivoxel pattern analyses. *J. Neurosci.* 33, 8549–8558. doi:10.1523/JNEUROSCI.1829-12.2013.
- Griffin, J.W., 2020. Quantifying the face inversion effect in nonhuman primates: a phylogenetic meta-analysis. *Anim. Cogn.* 23, 237–249. doi:10.1007/s10071-019-01340-8.
- Grill-Spector, K., Henson, R., Martin, A., 2006. Repetition and the brain: neural models of stimulus-specific effects. *Trends Cogn. Sci.* 10, 14–23. doi:10.1016/j.tics.2005.11.006.
- Grill-Spector, K., Malach, R., 2001. fMR-adaptation: a tool for studying the functional properties of human cortical neurons. *Acta Psychol. (Amst.)* 107, 293–321.
- Hancock, P.J.B., Bruce, V., Burton, A.M., 2000. Recognition of unfamiliar faces. *Trends Cogn. Sci.* 4, 330–337. doi:10.1016/S1364-6613(00)01519-9.
- Haxby, J.V., Ungerleider, L.G., Clark, V.P., Schouten, J.L., Hoffman, E.A., Martin, A., 1999. The effect of face inversion on activity in human neural systems for face and object perception. *Neuron* 22, 189–199.
- Hermann, P., Grotheer, M., Kovacs, G., Vidnyanszky, Z., 2017. The relationship between repetition suppression and face perception. *Brain Imaging Behav* 11, 1018–1028. doi:10.1007/s11682-016-9575-9.
- Hills, P.J., Lewis, M.B., 2018. The development of face expertise: evidence for a qualitative change in processing. *Cogn. Dev.* 48, 1–18. doi:10.1016/j.cogdev.2018.05.003.
- Hsiao, J.H., Cottrell, G., 2008. Two fixations suffice in face recognition. *Psychol. Sci.* 19, 998–1006. doi:10.1111/j.1467-9280.2008.02191.x.
- Hughes, B.L., Camp, N.P., Gomez, J., Natu, V.S., Grill-Spector, K., Eberhardt, J.L., 2019. Neural adaptation to faces reveals racial outgroup homogeneity effects in early perception. *Proc. Natl. Acad. Sci.* 116, 14532–14537. doi:10.1073/pnas.1822084116.
- Jacques, C., d'Arripe, O., Rossion, B., 2007. The time course of the inversion effect during individual face discrimination. *J. Vis.* 7 (8), 1–9. doi:10.1167/7.8.3.Introduction, 3.
- Jenkins, R., Dowsett, A.J., Burton, A.M., 2018. How many faces do people know? *Proc. Biol. Sci.* 285. doi:10.1098/rspb.2018.1319.
- Jonas, J., Brissart, H., Hossu, G., Colnat-Coulbois, S., Vignal, J.-P., Rossion, B., Maillard, L., 2018. A face identity hallucination (palinopsia) generated by intracerebral stimulation of the face-selective right lateral fusiform cortex. *Cortex* 99, 296–310. doi:10.1016/j.cortex.2017.11.022.
- Jonas, J., Descoins, M., Koessler, L., Colnat-Coulbois, S., Sauvée, M., Guye, M., Vignal, J.-P., Vespignani, H., Rossion, B., Maillard, L., 2012. Focal electrical intracerebral stimulation of a face-sensitive area causes transient prosopagnosia. *Neuroscience* 222, 281–288. doi:10.1016/j.neuroscience.2012.07.021.

- Jonas, J., Jacques, C., Liu-shuang, J., Brissart, H., Colnat-coulbois, S., Maillard, L., Rossion, B., 2016. A face-selective ventral occipito-temporal map of the human brain with intracerebral potentials. *Proc. Natl. Acad. Sci. U.S.A.* 113, E4088–E4097. doi:10.1073/pnas.1522033113.
- Jonas, J., Rossion, B., Brissart, H., Frismand, S., Jacques, C., Hossu, G., Colnat-Coulbois, S., Vespignani, H., Vignal, J.P., Maillard, L., 2015. Beyond the core face-processing network: Intracerebral stimulation of a face-selective area in the right anterior fusiform gyrus elicits transient prosopagnosia. *Cortex* 72, 140–155. doi:10.1016/j.cortex.2015.05.026.
- Jonas, J., Rossion, B., Krieg, J., Koessler, L., Colnat-Coulbois, S., Vespignani, H., Jacques, C., Vignal, J.P., Brissart, H., Maillard, L., 2014. Intracerebral electrical stimulation of a face-selective area in the right inferior occipital cortex impairs individual face discrimination. *Neuroimage* 99, 487–497. doi:10.1016/j.neuroimage.2014.06.017.
- Kanwisher, N., 2017. The Quest for the FFA and Where It Led. *J. Neurosci.* 37, 1056–1061. doi:10.1523/JNEUROSCI.1706-16.2016.
- Kanwisher, N., McDermott, J., Chun, M.M., 1997. The fusiform face area: a module in human extrastriate cortex specialized for face perception. *J. Neurosci.* 17, 4302–4311. doi:10.1098/Rstb.2006.1934.
- Kim, J.-J., Crespo-Facorro, B., Andreasen, N.C., O'Leary, D.S., Zhang, B., Harris, G., Magnotta, V.A., 2000. An MRI-Based Parcellation Method for the Temporal Lobe. *Neuroimage* 11, 271–288. doi:10.1006/nimg.2000.0543.
- Kriegeskorte, N., Formisano, E., Sorger, B., Goebel, R., 2007. Individual faces elicit distinct response patterns in human anterior temporal cortex. *Proc. Natl. Acad. Sci. U.S.A.* 104, 20600–20605.
- Lambon Ralph, M.A., 2014. Neurocognitive insights on conceptual knowledge and its breakdown. *Philos. Trans. R. Soc. Lond. B. Biol. Sci.* 369, 20120392. doi:10.1098/rstb.2012.0392.
- Leopold, D.A., Bondar, I.V., Giese, M.A., 2006. Norm-based face encoding by single neurons in the monkey inferotemporal cortex. *Nature* 442, 572–575. doi:10.1038/nature04951.
- Liu-Shuang, J., Norcia, A.M., Rossion, B., 2014. An objective index of individual face discrimination in the right occipito-temporal cortex by means of fast periodic oddball stimulation. *Neuropsychologia* 52, 57–72. doi:10.1016/j.neuropsychologia.2013.10.022.
- Liu-Shuang, J., Torfs, K., Rossion, B., 2016. An objective electrophysiological marker of face individualisation impairment in acquired prosopagnosia with fast periodic visual stimulation. *Neuropsychologia* 83, 100–113. doi:10.1016/j.neuropsychologia.2015.08.023.
- Lochy, A., Jacques, C., Maillard, L., Colnat-Coulbois, S., Rossion, B., Jonas, J., 2018. Selective visual representation of letters and words in the left ventral occipito-temporal cortex with intracerebral recordings. *Proc. Natl. Acad. Sci. U.S.A.* 115, E7595–E7604. doi:10.1073/pnas.1718987115.
- Mazard, A., Schiltz, C., Rossion, B., 2006. Recovery from adaptation to facial identity is larger for upright than inverted faces in the human occipito-temporal cortex. *Neuropsychologia* 44, 912–922. doi:10.1016/j.neuropsychologia.2005.08.015.
- Meadows, J.C., 1974. The anatomical basis of prosopagnosia. *J. Neurol. Neurosurg. Psychiatry*.
- Megreya, A.M., Burton, A.M., 2006. Unfamiliar faces are not faces: Evidence from a matching task. *Mem. Cognit.* 34, 865–876. doi:10.3758/BF03193433.
- Mogi, T., Tsunoda, T., Yoshino, A., 2019. Altered upright face recognition and presence of face inversion effect in temporal lobe epilepsy: an event-related potential study. *Psychiatry Clin. Neurosci.* 73, 269–276. doi:10.1111/pcn.12829.
- Murphy, J., Gray, K.L.H., Cook, R., 2020. Inverted faces benefit from whole-face processing. *Cognition* 194, 104105. doi:10.1016/j.cognition.2019.104105.
- Natu, V.S., Jiang, F., Narvekar, A., Keshvari, S., Blanz, V., O'Toole, A.J., 2010. Dissociable neural patterns of facial identity across changes in viewpoint. *J. Cogn. Neurosci.* 22, 1570–1582. doi:10.1162/jocn.2009.21312.
- Nestor, A., Plaut, D.C., Behrmann, M., 2016. Feature-based face representations and image reconstruction from behavioral and neural data. *Proc. Natl. Acad. Sci. U. S. A.* 113, 416–421. doi:10.1073/pnas.1514551112.
- Nestor, A., Plaut, D.C., Behrmann, M., 2011. Unraveling the distributed neural code of facial identity through spatiotemporal pattern analysis. *Proc. Natl. Acad. Sci. U.S.A.* 108, 9998–10003. doi:10.1073/pnas.1102433108.
- Newport, C., Wallis, G., Reshitnyk, Y., Siebeck, U.E., 2016. Discrimination of human faces by archerfish (*Toxotes chatareus*). *Sci. Rep.* 6, 27523. doi:10.1038/srep27523.
- O'Toole, A.J., Jiang, F., Roark, D., Abdi, H., 2006. Predicting human performance for face recognition. In: *Chellappa, R., Zhao, W. (Eds.), Face Processing: Advanced Models and Methods*. Academic Press, New York, pp. 293–320.
- Palermo, R., Rhodes, G., 2007. Are you always on my mind? A review of how face perception and attention interact. *Neuropsychologia* 45, 75–92. doi:10.1016/j.neuropsychologia.2006.04.025.
- Parr, L.A., Heintz, M., Pradhan, G., 2008. Rhesus monkeys (*Macaca mulatta*) lack expertise in face processing. *J. Comp. Psychol.* 122, 390–402. doi:10.1037/0735-7036.122.4.390.
- Pinsk, M.A., Arcaro, M., Weiner, K.S., Kalkus, J.F., Inati, S.J., Gross, C.G., Kastner, S., 2009. Neural representations of faces and body parts in macaque and human cortex: a comparative fMRI study. *J. Neurophysiol.* 101, 2581–2600. doi:10.1152/jn.91198.2008.
- Pitcher, D., Duchaine, B., Walsh, V., Yovel, G., Kanwisher, N., 2011a. The role of lateral occipital face and object areas in the face inversion effect. *Neuropsychologia* 49, 3448–3453. doi:10.1016/j.neuropsychologia.2011.08.020.
- Pitcher, D., Walsh, V., Duchaine, B., 2011b. The role of the occipital face area in the cortical face perception network. *Exp. Brain Res.* 209, 481–493. doi:10.1007/s00221-011-2579-1.
- Pitcher, D., Walsh, V., Yovel, G., Duchaine, B., 2007. TMS evidence for the involvement of the right occipital face area in early face processing. *Curr. Biol.* 17, 1568–1573. doi:10.1016/j.cub.2007.07.063.
- Puce, A., Allison, T., McCarthy, G., 1999. Electrophysiological studies of human face perception. III: effects of top-down processing on face-specific potentials. *Cereb. Cortex* 9, 445–458.
- Quian Quiroga, R., 2012. Concept cells: the building blocks of declarative memory functions. *Nat. Rev. Neurosci.* 13, 587–597. doi:10.1038/nrn3251.
- Quian Quiroga, R., Reddy, L., Kreiman, G., Koch, C., Fried, I., 2005. Invariant visual representation by single neurons in the human brain. *Nature* 435, 1102–1107. doi:10.1038/nature03687.
- Rajimehr, R., Young, J.C., Tootell, R.B.H., 2009. An anterior temporal face patch in human cortex, predicted by macaque maps. *Proc. Natl. Acad. Sci. U.S.A.* 106, 1995–2000. doi:10.1073/pnas.0807304106.
- Ramirez, F.M., 2018. Orientation Encoding and Viewpoint Invariance in Face Recognition: inferring Neural Properties from Large-Scale Signals. *Neuroscientist* 24, 582–608. doi:10.1177/1073858418769554.
- Rey, H.G., Gori, B., Chauré, F.J., Collavini, S., Blenkmann, A.O., Seoane, P., Seoane, E., Kochen, S., Quian Quiroga, R., 2020. Single neuron coding of identity in the human hippocampal formation. *Curr. Biol.* 30, 1152–1159. doi:10.1016/j.cub.2020.01.035, e3.
- Rice, G.E., Caswell, H., Moore, P., Hoffman, P., Lambon Ralph, M.A., 2018. The roles of left versus right anterior temporal lobes in semantic memory: a neuropsychological comparison of postsurgical temporal lobe epilepsy patients. *Cereb. Cortex* 28, 1487–1501. doi:10.1093/cercor/bhx362.
- Riley, J.D., Fling, B.W., Cramer, S.C., Lin, J.J., 2015. Altered organization of face-processing networks in temporal lobe epilepsy. *Epilepsia* 56, 762–771. doi:10.1111/epi.12976.
- Rosenthal, G., Sporns, O., Avidan, G., 2016. Stimulus dependent dynamic reorganization of the human face processing network. *Cereb. Cortex* 27, 4823–4834. doi:10.1093/cercor/bhw279.
- Rossion, B., Retter, T.L., Liu-Shuang, J., 2020. Understanding human individuation of unfamiliar faces with oddball fast periodic visual stimulation and electroencephalography. *Eur J Neurosci*. Accepted Author Manuscript. doi:10.1111/ejn.14865.
- Rossion, B., 2018. Damasio's error - Prosopagnosia with intact within-category object recognition. *J. Neuropsychol.* 12, 357–388. doi:10.1111/jnp.12162.
- Rossion, B., 2014. Understanding face perception by means of prosopagnosia and neuroimaging. *Front. Biosci. Elit.* 6, 258–307.
- Rossion, B., 2008. Picture-plane inversion leads to qualitative changes of face perception. *Acta Psychol. (Amst)*. 128, 274–289. doi:10.1016/j.actpsy.2008.02.003.
- Rossion, B., Jacques, C., Jonas, J., 2018. Mapping face categorization in the human ventral occipito-temporal cortex with direct neural intracranial recordings. *Ann. N.Y. Acad. Sci.* doi:10.1111/nyas.13596.
- Rossion, B., Michel, C., 2018. Normative accuracy and response time data for the computerized Benton Facial Recognition Test (BFRT-c). *Behav. Res. Methods* 50, 2442–2460. doi:10.3758/s13428-018-1023-x.
- Rossion, B., Schiltz, C., Robaye, L., Pirenne, D., Crommelinck, M., 2001. How does the brain discriminate familiar and unfamiliar faces?: a PET study of face categorical perception. *J. Cogn. Neurosci.* 13, 1019–1034. doi:10.1162/089992901753165917.
- Rossion, B., Taubert, J., 2019. What can we learn about human individual face recognition from experimental studies in monkeys? *Vision Res.* 157, 142–158. doi:10.1016/j.visres.2018.03.012.
- Rostalski, S.-M., Amado, C., Kovács, G., 2019. Repetition suppression for noisy and intact faces in the occipito-temporal cortex. *Front. Psychol.* 10, 1348. doi:10.3389/fpsyg.2019.01348.
- Salado, A.L., Koessler, L., De Mijolla, G., Schmitt, E., Vignal, J.-P., Civit, T., Tyvaert, L., Jonas, J., Maillard, L.G., Colnat-Coulbois, S., 2018. sEEG is a safe procedure for a comprehensive anatomic exploration of the insula: a retrospective study of 108 procedures representing 254 transopercular insular electrodes. *Oper. Neurosurg.* 14, 1–8. doi:10.1093/ons/opx106.
- Schiltz, C., Rossion, B., 2006. Faces are represented holistically in the human occipito-temporal cortex. *Neuroimage* 32, 1385–1394. doi:10.1016/j.neuroimage.2006.05.037.
- Schretlen, D.J., Pearlson, G.D., Anthony, J.C., Yates, K.O., 2001. Determinants of benton facial recognition test performance in normal adults. *Neuropsychology*. doi:10.1037/0894-4105.15.3.405.
- Sekuler, A.B., Gaspar, C.M., Gold, J.M., Bennett, P.J., 2004. Inversion leads to quantitative, not qualitative, changes in face processing. *Curr. Biol.* 14, 391–396.
- Sergent, J., Signoret, J.L., 1992. Functional and anatomical decomposition of face processing - evidence from prosopagnosia and pet study of normal subjects. *Philos. Trans. R. Soc. London Ser. B-Biological Sci.* 335, 55–62.
- Sheehan, M.J., Nachman, M.W., 2014. Morphological and population genomic evidence that human faces have evolved to signal individual identity. *Nat. Commun.* 5, 4800. doi:10.1038/ncomms5800.
- Sheehan, M.J., Tibbetts, E.A., 2011. Specialized face learning is associated with individual recognition in paper wasps. *Science* 334 (80–), 1272–1275. doi:10.1126/science.1211334.
- Talairach, J., Bancaud, J., 1973. Stereotaxic approach to epilepsy. Methodology of anatomo-functional stereotaxic investigations. *Prog. Neurol. Surg.* 5, 297–354. doi:10.1159/000394343.
- Tarr, M.J., Bühlhoff, H.H., 1998. Image-based object recognition in man, monkey and machine. *Cognition* 67, 1–20.
- Verosky, S.C., Zoner, K.A., Marble, C.W., Sammon, M.M., Babarinsa, C.O., 2020. Familiarization increases face individuation measured with fast periodic visual stimulation. *Biol. Psychol.* 153, 107883. doi:10.1016/j.biopsycho.2020.107883.
- Von Der Heide, R.J., Skipper, L.M., Olson, I.R., 2013. Anterior temporal face patches:

- a meta-analysis and empirical study. *Front. Hum. Neurosci.* 7, 17. doi:10.3389/fnhum.2013.00017.
- Wandell, B.A., 2011. The neurobiological basis of seeing words. *Ann. N.Y. Acad. Sci.* 1224, 63–80. doi:10.1111/j.1749-6632.2010.05954.x.
- Weiner, K.S., Golarai, G., Caspers, J., Chuapoco, M.R., Mohlberg, H., Zilles, K., Amunts, K., Grill-Spector, K., 2014. The mid-fusiform sulcus: a landmark identifying both cytoarchitectonic and functional divisions of human ventral temporal cortex. *Neuroimage* 84, 453–465. doi:10.1016/j.neuroimage.2013.08.068.
- Weiner, K.S., Grill-Spector, K., 2012. The improbable simplicity of the fusiform face area. *Trends Cogn. Sci.* 16, 251–254. doi:10.1016/j.tics.2012.03.003.
- Yan, X., Liu-Shuang, J., Rossion, B., 2019. Effect of face-related task on rapid individual face discrimination. *Neuropsychologia* 129, 236–245. doi:10.1016/j.neuropsychologia.2019.04.002.
- Yin, R.K., 1969. Looking at upside-down faces. *J. Exp. Psychol. Percept. Perform.* 81, 141–145.
- Young, M.P., Yamane, S., 1992. Sparse Population Coding of Faces in the Inferotemporal Cortex. *Science* 256 (80–), 1327–1331.
- Yovel, G., Kanwisher, N., 2005. The neural basis of the behavioral face-inversion effect. *Curr. Biol.* 15, 2256–2262.
- Zhen, Z., Yang, Z., Huang, L., Kong, X., Wang, X., Dang, X., Huang, Y., Song, Y., Liu, J., 2015. Quantifying interindividual variability and asymmetry of face-selective regions: a probabilistic functional atlas. *Neuroimage* 113, 13–25. doi:10.1016/j.neuroimage.2015.03.010.